IAI Journals.ASM.org

Transcriptional Analysis of the MrpJ Network: Modulation of Diverse Virulence-Associated Genes and Direct Regulation of *mrp* Fimbrial and *flhDC* Flagellar Operons in *Proteus mirabilis*

Nadine J. Bode, Irina Debnath, Lisa Kuan, Anjelique Schulfer, Maureen Ty, Melanie M. Pearson

Department of Microbiology, New York University Medical Center, New York, New York, USA

The enteric bacterium *Proteus mirabilis* is associated with a significant number of catheter-associated urinary tract infections (UTIs). Strict regulation of the antagonistic processes of adhesion and motility, mediated by fimbriae and flagella, respectively, is essential for disease progression. Previously, the transcriptional regulator MrpJ, which is encoded by the *mrp* fimbrial operon, has been shown to repress both swimming and swarming motility. Here we show that MrpJ affects an array of cellular processes beyond adherence and motility. Microarray analysis found that expression of *mrpJ* mimicking levels observed during UTIs leads to differential expression of 217 genes related to, among other functions, bacterial virulence, type VI secretion, and metabolism. We probed the molecular mechanism of transcriptional regulation by MrpJ using transcriptional reporters and chromatin immunoprecipitation (ChIP). Binding of MrpJ to two virulence-associated target gene promoters, the promoters of the flagellar master regulator *flhDC* and *mrp* itself, appears to be affected by the condensation state of the native chromosome, although both targets share a direct MrpJ binding site proximal to the transcriptional start. Furthermore, an *mrpJ* deletion mutant colonized the bladders of mice at significantly lower levels in a transurethral model of infection. Additionally, we observed that *mrpJ* is widely conserved in a collection of recent clinical isolates. Altogether, these findings support a role of MrpJ as a global regulator of *P. mirabilis* virulence.

Bacterial pathogens utilize a myriad of complex regulatory networks to adapt gene expression in response to environmental cues encountered in the host. Trying to walk a fine balance of avoiding detection by the host immune system, while ensuring acquisition of all essential nutrients and promoting growth, bacteria employ transcriptional and posttranscriptional strategies to combat the host's defenses. A prominent example is the specific induction of iron and zinc uptake systems during infection, regulated by Fur and Zur, respectively, which allows pathogens to gain access to these essential transition metals in the restricted host environment (1, 2).

Urinary tract infections (UTIs) are among the most common bacterial infections (3), presenting a significant public health burden amounting to annual costs of about 3.5 billion dollars in the United States alone (4). Although *Proteus mirabilis* causes a relatively small proportion of UTIs in healthy individuals, it is a common cause of cystitis and pyelonephritis in individuals with indwelling catheters or anatomical abnormalities of the urinary tract (4, 5).

UTIs occur almost exclusively in an ascending route, meaning that bacteria of fecal origin gain entry to the bladder via the urethra and then spread to the kidneys via the ureters (4). Initially, bacteria adhere to host epithelial cells via proteinaceous supramolecular structures referred to as fimbriae (or pili) (6), which allow pathogens to withstand the mechanical flow of urine (5). Later in infection, bacteria can move into the kidneys using the force created by rotational movement of peritrichous flagella (7).

Flagellum-mediated motility and adhesion through fimbriae are inherently opposing processes that underlie tight regulation to allow a productive infection to take place. Sequencing of the first *P. mirabilis* genome in 2008 (8) revealed the presence of 17 potential chaperone-usher fimbriae. To date, biological evidence for the production of seven of these has been collected (9–16). Among these, the best studied is the mannose-resistant *Proteus*-like (MR/P) fimbria, which has been shown to be an important virulence factor that contributes to colonization of the urinary tract in a murine model of infection (17), as well as affecting the localization of bacteria within the bladder (18). In fact, all mutants defective in MR/P fimbria assembly tested thus far are attenuated for virulence in experimental UTIs (19–22). Expression of MR/P fimbriae undergoes phase variation: the *mrp* promoter contains an invertible element flanked by inverted repeat sequences, and the orientation of this element strictly regulates transcription of the fimbrial operon (20, 23). Transcribed at low levels in culture, the genes of the *mrp* operon show the largest fold induction of all *P. mirabilis* genes *in vivo* (24). Consequently, the major fimbrial subunit MrpA, as well as the tip adhesin MrpH, have been the subjects of multiple vaccine efforts (25–31). Recent work illustrates that *mrpA* is present in 96% of a collection of 48 clinical *P.*

Received 21 November 2014 **Returned for modification** 25 December 2014
Accepted 29 March 2015

Accepted manuscript posted online 6 April 2015

Citation Bode NJ, Debnath I, Kuan L, Schulfer A, Ty M, Pearson MM. 2015. Transcriptional analysis of the MrpJ network: modulation of diverse virulence-associated genes and direct regulation of *mrp* fimbrial and *flhDC* flagellar operons in *Proteus mirabilis*. Infect Immun 83:2542–2556. doi:10.1128/IAI.02978-14.

Editor: S. M. Payne

Address correspondence to Melanie M. Pearson, Melanie.Pearson@nyumc.org.

N.J.B. and I.D. contributed equally to this work.

Supplemental material for this article may be found at http://dx.doi.org/10.1128/IAI.02978-14.

doi:10.1128/IAI.02978-14

mirabilis isolates collected in 2012, as well as all seven sequenced genomes available at the time (13).

MrpJ, a transcriptional regulator encoded by the last gene of the MR/P fimbrial operon (32), has previously been shown to repress both swarming and swimming motility in *P. mirabilis*, permitting the bacteria to reciprocally control motility and adherence when *mrp* is expressed (32, 33). This helix-turn-helix (HTH) xenobiotic response element (XRE) family member interacts directly with the promoter of the flagellar master regulator *flhDC* (33). PapX, a functional homolog of MrpJ associated with P fimbriae in uropathogenic *Escherichia coli* (UPEC) similarly represses motility (34, 35). Recently, FmrA has been identified as a novel fimbria-associated regulator of motility in Shiga toxin-producing *E. coli* O157:H7 (36). Homologs of *mrpJ* have been reported in the *Enterobacteriaceae* species *Photorhabdus temperata* (37) and *Xenorhabdus nematophila* (38), although their function remains to be elucidated. BLAST searches reveal *mrpJ* homologs in at least 20 bacterial species. They are frequently associated with fimbrial operons in *Proteus* and *Providencia* spp., and *P. mirabilis* reference strain HI4320 carries 14 *mrpJ* paralogs in addition to *mrpJ* itself (33).

This study closely examines the role of MrpJ as an important regulator of motility and adherence in the uropathogen *P. mirabilis*. Transcriptomic data reveal a complex network of genes affected by *mrpJ* expression, many of which have previously been associated with virulence. We demonstrate that MrpJ has positive autoregulatory function using *in vitro* reporter assays that allow us to define an MrpJ-responsive fragment of the *mrp* promoter. Utilizing chromatin immunoprecipitation (ChIP), we extend our observations to the native state of the bacterial chromosome, confirming direct interactions of MrpJ with the *mrp* and *flhDC* promoters. Coupled with the attenuation of the *mrpJ* mutant observed in the murine UTI challenge *in vivo*, our results elucidate significant novel aspects of this important transcriptional regulator with regard to *P. mirabilis* virulence.

MATERIALS AND METHODS

Bacterial strains, plasmids, and media. All bacterial strains and plasmids used in this study are listed in Table S1 in the supplemental material. The New York University (NYU) clinical isolate collection and 10 nursing home isolates used for the *mrpJ* PCR survey have been previously described (13). All strains were grown at 37°C in low-salt nonswarming Luria broth (LB) (per liter, 10 g tryptone, 5 g yeast extract, 0.5 g NaCl) or on LB medium solidified with 1.5% agar. The following antibiotics were supplied at the indicated concentrations when necessary: ampicillin (100 μg/ml), gentamicin (15 μg/ml), and kanamycin (25 μg/ml). Transformants of *P. mirabilis* Φ(*mrpAp-lacZ*) operon fusion strains with pLX3607 or pLX3805 were selected on LB agar with 25 to 50 μg/ml ampicillin but subsequently maintained using 100 μg/ml ampicillin.

To construct the arabinose-inducible His_6-tagged *mrpJ* vector used in chromatin immunoprecipitation (ChIP) experiments, a fragment containing *mrpJ* was PCR amplified from pLX2501 (32) using primers QE60Nco and QE60Hind. The resulting amplicon was digested with NcoI, which cuts at the 5′ insertion site for *mrpJ* coding sequence, and ligated into pBAD/*Myc*-HisA (Life Technologies) which had been linearized with NcoI and PmeI, resulting in plasmid pMP190.

All primer sequences are described in Table S2 in the supplemental material.

Identification of *mrpJ* in sequenced genomes and clinical isolates. BLAST (39) was used to identify *mrpJ* in the 14 *P. mirabilis* genomes currently available in GenBank (strains HI4320, BB2000, PR03, C05028, ATCC 29906, ATCC 7002, WGLW4, WGLW6, Pm-Oxa48, and FDA_MicroDB strains 60, 67, 86, 87, and 91) (8, 40–43). PCR with *mrpJ*-specific primers was used to determine the presence of *mrpJ* in a clinical isolate collection (13). To determine whether *mrpJ* was part of the *mrp* operon in *mrpA*-negative strain NYU014, we used *mrpH*- and *mrpJ*-specific primers mrpH-seqF and mrpJ-RTR.

Microarrays. The *P. mirabilis* HI4320 microarray has been described previously (44). To measure MrpJ-regulated gene transcription, *P. mirabilis* HI4320, HI4320Δ*mrpJ*, vector control HI4320(pLX3607), or *mrpJ in vivo* mimic HI4320(pLX3805) were cultured to logarithmic phase with aeration (optical density at 600 nm [OD_{600}] of 0.7 to 0.9). Briefly, RNA was stabilized with RNAprotect (Qiagen) and isolated from cultures using the RNeasy minikit (Qiagen) according to the manufacturer's directions, with the exception of treating stabilized bacteria with 3 mg/ml lysozyme in Tris-EDTA (TE) buffer for 15 min. RNA was used as a cDNA template and labeled with either cyanine 3 or cyanine 5 dye as previously described (44) before microarray hybridization. Slides were scanned with a ScanArray Express microarray scanner (PerkinElmer) at 10-μm resolution, and data were analyzed using MeV software (v. 4.7.4; J. Craig Venter Institute). Four independent microarrays were analyzed for each condition.

qRT-PCR. RNA from logarithmic-phase, aerated broth cultures of *P. mirabilis* (microarray validation) or aerated broth cultures of *P. mirabilis* with an OD_{600} of 2 (ChIP validation) was used as the template for cDNA synthesis using the Superscript first-strand synthesis system (Life Technologies) according to the manufacturer's protocol. Quantitative reverse transcriptase PCR (qRT-PCR) was performed as previously described (44), with two modifications: the 2× PCR master mix was either SsoAdvanced Universal SYBR green (Bio-Rad; microarray validation) or Maxima SYBR green (Thermo Scientific; ChIP validation), and the thermal cycler was a CFX Connect real-time system (Bio-Rad).

Determination of the transcriptional start site. The 5′ rapid amplification of cDNA ends (5′ RACE) system (Life Technologies) was used to identify the transcriptional start site for the *mrpABCDEFGHJ* and *flhDC* operons according to the manufacturer's protocol. Amplicons were cloned, and full-length clones were sequenced. Four (*mrp*) or five (*flh*) identical clones were used to localize the transcriptional +1 site.

Construction of transcriptional fusions to *lacZ*. *lacZ* was amplified from the operon fusion vector pRS415 using Q5 High-Fidelity polymerase (NEB) and cloned into XhoI/KpnI-HF-digested pUC18R6K-mini-Tn*7*T-Gm to form pNB022. Transformants were streaked on LB-gentamicin (LB plus gentamicin) plates supplemented with 5-bromo-4-chloro-3-indolyl-β-D-galactopyranoside (X-Gal) (40 μg/ml), and isolates showing the blue color indicative of LacZ activity were selected. Sequencing (GENEWIZ Inc.) confirmed that amplified regulatory elements upstream of *lacZ* were maintained without error.

5′ truncated promoter fragments of *mrpA* were generated by PCR from *P. mirabilis* HI4320 genomic DNA using a common reverse primer and forward primers that anneal to various distances upstream. The resulting fragments were cloned into the XhoI and NotI sites of pNB022. Forward primers NB75 to NB78 specifically anneal to the *mrp* promoter invertible element (IE) in the on direction. Promoter fragments that contain the full IE (amplified using forward primers NB65, NB66, and NB90) were confirmed to be in the on orientation. All plasmids were sequenced to verify the correct sequence of the cloned inserts (using primers NB52 and NB60).

A method by Choi et al. was adapted to construct single-copy operon fusions integrated into the HI4320 *att*Tn*7* locus downstream of *glmS* (45). Briefly, strain HI4320 with the IE locked in the OFF orientation (MR/P L-OFF) was transformed with 100 to 200 ng of plasmid carrying a Φ(*mrpAp-lacZ*) operon fusion and the transposase expression vector pTNS3. Cells were recovered in LB medium for 1 h postelectroporation. Gentamicin-resistant transformants were screened for successful integration at the *glmS att*Tn*7* site by colony PCR as described previously (45). A second PCR using primers specific to the secondary *att*Tn*7* site in *carA* (45) was performed at all times to ensure that no double integration event had taken place. Following purification of a single colony, chromosomal

DNA was extracted from a liquid overnight culture using the QIAamp DNA minikit (Qiagen) according to the instructions of the manufacturer. Using primers annealing to the flanking region of the two *att*Tn*7* loci (JS72/Tn7rev and JS73/NB46), a second PCR was performed with *Taq* DNA polymerase (NEB). The cycle conditions for the second PCR were as follows: (i) 5 min at 95°C; (ii) 30 cycles, with 1 cycle consisting of 30 s at 94°C, 40 s at 61°C, and 8 min at 68°C; and (iii) 10 min at 72°C. Successful integration resulted in an observable size shift of the amplified fragment, corresponding to the length of the transformed mini-Tn*7* derivative.

β-Galactosidase assay. To determine the effect of MrpJ overproduction on the expression of Φ(*mrpAp-lacZ*) transcriptional fusions, saturated overnight cultures were diluted to a starting OD_{600} of approximately 0.04 in 5 ml LB supplied with ampicillin. The cultures were incubated in a shaker incubator at 37°C and 225 rpm until mid-logarithmic growth phase (OD_{600} of 0.7 to 0.9), when the cells were harvested by centrifugation and washed in 0.88% NaCl prior to enzymatic assays.

Bacteria were permeabilized by the addition of chloroform and sodium dodecyl sulfate, and LacZ activity was measured as described previously (46). All assays were performed at room temperature (approximately 21°C). Activities are expressed in arbitrary Miller units (47). Individual cultures were assessed in duplicate, and graphed values represent the averages from four biologically independent experiments and the corresponding standard deviations (SD).

Immunoblot analysis. Protein samples were separated by SDS-PAGE. Western blot analysis was conducted using penta-His antibody (anti-His_5; Qiagen) (1:4,000 dilution in phosphate-buffered saline [PBS] with 3% bovine serum albumin [BSA]) and peroxide-conjugated goat anti-mouse IgG (Bio-Rad) secondary antibodies. Western blots were developed using ECL Plus Western blotting detection system (Thermo Scientific) according to the manufacturer's protocol. Each gel was run in duplicate, followed by Coomassie blue staining to control for loading.

Bacterial ChIP and promoter walk. The bacterial ChIP protocol was developed for *P. mirabilis* and was guided by published protocols (48–50) (see supplemental material for the detailed method). Briefly, *P. mirabilis* cells were cross-linked by formaldehyde, DNA-protein complexes were sheared by sonication, and His_6-tagged MrpJ was immunoprecipitated with anti-His_5 antibody. Next, the immunoprecipitated targets were stringently washed to remove nonspecific background, heat treated at 65°C to reverse cross-linking and column purified. PCR was used to analyze MrpJ-DNA interaction with *mrpA* and *flhD* upstream regulatory elements.

We designed a ChIP-PCR primer set to target a previously published positive electrophoretic mobility shift assay (EMSA) probe region (33) of the *flhD* promoter (fragment "j") to confirm the successful immunoprecipitation (IP) of MrpJ-bound DNA complexes. A no-antibody bead-only control, an immunoprecipitation of a vector control and *rpoA* PCR as a nonspecific target gene control were included in each ChIP assay and in their downstream analysis. ChIP-PCR of MrpJ-bound DNA complexes was quantified using Image Studio software (LI-COR).

Mouse model of UTI. Five- to 6-week-old female CBA/J mice (Jackson Laboratory) were transurethrally inoculated with *P. mirabilis* in accordance with NYU Langone Medical Center (NYULMC) IACUC-approved animal protocol number 140204. The infection procedure was carried out with some modifications of a published protocol (24, 51). Specifically, overnight cultures of wild-type *P. mirabilis* HI4320 and the isogenic *mrpJ* mutant (32) were adjusted to an estimated density of 2×10^8 CFU/ml (OD_{600} of 0.2). Mice were then infected with 50 μl of this culture (1×10^7 CFU) via a transurethral sterile polyethylene catheter attached to an infusion pump (Harvard Apparatus), after being anesthetized by intraperitoneal injection of anesthetic. Seven days postinfection, urine was collected by gentle abdominal massage, and then organs (bladders, kidneys, and spleens) were harvested aseptically, weighed, and homogenized in sterile 1× PBS. Bacterial titers were determined by plating serial dilutions of homogenates or urine samples on agar plates. The limit of detection was set at 200 CFU g^{-1} tissue for homogenate samples with undetectable colony numbers.

Statistical analysis. Statistical significance of qRT-PCR data was calculated using a one-sample *t* test and a theoretical mean of 1.0. Significance of β-galactosidase activity and ChIP complex enrichment was calculated using Student's *t* test. The Mann-Whitney U test was used to analyze the results from animal experiments. Graphing and analysis were performed using Prism software (v. 6.0f; GraphPad).

Microarray data accession number. The data from the microarray experiments are available at GEO accession number GSE63321.

RESULTS

MrpJ is present across diverse *P. mirabilis* isolates. We recently reported that *mrpA* is highly conserved in a collection of 65 *P. mirabilis* strains, including 7 sequenced genomes, 10 nursing home urinary catheter isolates collected in the early 1980s, and 48 recent isolates from NYU Tisch Hospital (62/65 strains [95%]) (13). To determine whether *mrpJ* is similarly widespread, we examined the same strains by PCR or sequence analysis. We detected *mrpJ* in 63/65 (97%) of these strains. All strains that were positive for *mrpA* were also positive for *mrpJ*. Interestingly, the NYU014 strain was PCR negative for *mrpA* but positive for *mrpJ*; however, an amplicon that bridged *mrpH* and *mrpJ* was obtained. As this strain is also negative for MR/P-type hemagglutination (data not shown), its *mrp* operon is possibly cryptic. In addition, *mrpJ* is located at the end of the *mrp* operon in all 14 *P. mirabilis* genomes currently searchable by BLAST (see Materials and Methods). Alignment of these 14 sequences revealed synonymous mutations in 6/333 nucleotides (1.8%), and one nonsynonymous change (P to L) found only in FDA_MicroDB_91.

MrpJ regulates virulence factors in addition to flagella. MrpJ has previously been shown to repress swimming and swarming motility by binding the promoter of the master regulator of flagella, *flhDC* (32, 33). Additional evidence suggested that MrpJ autoregulates the *mrp* operon: a Δ*mrpJ* mutant produces less MrpA protein (32). Furthermore, when viewed by transmission electron microscopy, *P. mirabilis* overexpressing *mrpJ* or *mrpJ* paralogs produce fimbriae with distinct appearances (33). To define the breadth of the MrpJ regulon, we used microarray analysis of *P. mirabilis* with various levels of *mrpJ* expression. Two sets of microarray experiments were conducted: wild-type strain HI4320 versus HI4320Δ*mrpJ* and strain HI4320 carrying an empty vector (pLX3607) versus HI4320 with *mrpJ* under an isopropyl-β-D-thiogalactopyranoside (IPTG)-inducible promoter (pLX3805). We expressed *mrpJ* in *trans* because the highest levels of expression measured thus far for this gene occur during UTIs, and *mrpJ* is expressed only at low levels *in vitro*. The amount of *mrpJ* transcript in mid-logarithmic-phase culture resulting from uninduced pLX3805 (2,178-fold median increase versus vector control) is comparable to the amount detected in the urine of mice experimentally infected with *P. mirabilis* 1 day postinfection (1,103-fold compared to *in vitro* broth control), and therefore, this strain may be considered an *in vivo* mimic for *mrpJ* (24).

We found many genes were differentially regulated at least 2-fold by MrpJ (Fig. 1). Specifically, during expression of *mrpJ* at levels comparable to those during infection, 70 genes were induced and 147 genes were repressed compared to the vector control (Tables 1 and 2, with complete results in Tables S3 and S4 in the supplemental material). In the Δ*mrpJ* strain, 13 genes were induced and 56 genes were repressed compared to the wild type (Tables S5 and S6). The amount of regulation in the Δ*mrpJ* strain

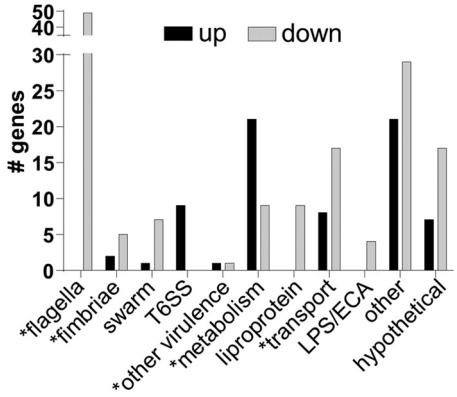

FIG 1 Categories of genes regulated by MrpJ. A vector control was compared to *mrpJ* expressed in *trans* at levels comparable to those during experimental UTIs, and differential transcription was measured by microarray. Gene classes that have previously been shown to contribute to *P. mirabilis* pathogenesis are indicated by an asterisk. ECA, enterobacterial common antigen.

compared to the wild type was relatively modest with the exception of *mrpA*, which was repressed 146.93-fold. This was not surprising, given that *mrpJ* is not expressed well *in vitro* (32).

As expected in the presence of *mrpJ*, flagellar genes were repressed: these genes included *flhDC* (−5.16- and −6.25-fold, respectively), which encodes the master regulator of flagella. In addition, swarming regulators *umoA* and *umoB* were repressed by MrpJ (−222- and −2.68-fold, respectively), while *lrhA* was induced (2.21-fold) (44, 52, 53), indicating that MrpJ not only represses motility but also interferes with swarmer cell differentiation. The cell shape-determining gene *ccm*, also implicated in swarming behavior (54), was the most repressed gene in the *in vivo* mimic strain (630-fold). The polyamine putrescine has also been found to contribute to swarming (55), and we found MrpJ repression of *speF* (−3.75-fold), which catalyzes the production of putrescine from ornithine.

Also consistent with previously published evidence that suggested an altered fimbrial profile when *mrpJ* was overexpressed (33), we found that several fimbrial operons were regulated by *mrpJ*: *pmfA*, *fim8A*, and *fim14A* were repressed, while the *mrp* operon itself was induced (−3.14-, −234-, −20.5-, and 12.3-fold, respectively). Three of these fimbriae, MR/P, PMF (*P. mirabilis* fimbria), and Fim14, have previously been shown to contribute to virulence in a mouse model of UTI (15, 19–22, 56, 57). In addition to regulation of anticipated systems, we found that MrpJ regulates other established virulence genes encoding the Pta toxin (2.25-fold) and ZapA protease (−14.3-fold) (58, 59). Furthermore, MrpJ regulated genes that could be associated with virulence or immune evasion, such as lipopolysaccharide (LPS) modifications (*pagP*, *lpxK*, and *msbB*; −5.01-, −2.21-, and −2.94-fold, respectively). A type VI secretion system (T6SS), including effector genes *idsA* and PMI0750 as well as seven genes in the operon which encodes the structural proteins of the T6SS (PMI0749-0734) (60–62), was induced by MrpJ. Thus, MrpJ regulates a variety of genes that are known or hypothesized to contribute to pathogenesis. These data, combined with the fact that *mrpJ* is strongly induced during experimental UTI, suggest that MrpJ is a master regulator of virulence.

Microarray data were validated by measuring transcript levels of selected genes by qRT-PCR (Fig. 2A; see Fig. S1 in the supple-

TABLE 1 Top 50 genes repressed in *mrpJ* overexpression strain compared to the vector control

ORF[a]	Gene	Annotation	Fold change
PMI1961	*ccm*	Putative membrane protein (Ccm1 protein)	−630.29
PMI1635	*fliK*	Flagellar hook length control protein	−509.87
PMI1652	*flgD*	Basal body rod modification protein	−469.29
PMI1631	*fliG*	Flagellar motor switch protein	−467.90
PMI1647	*flgI*	Flagellar P-ring protein precursor (basal body P-ring protein)	−466.93
PMI1637	*fliM*	Flagellar motor switch protein	−450.58
PMI1639	*fliO*	Flagellar protein	−441.62
PMI1670	*motA*	Chemotaxis protein (motility protein A)	−435.30
PMI1632	*fliH*	Flagellar assembly protein	−398.84
PMI1660	*flhB*	Flagellar biosynthetic protein	−341.98
PMI1654	*flgB*	Flagellar basal body rod protein	−329.89
PMI1618	*fliA*	RNA polymerase sigma factor for flagellar operon	−320.62
PMI1659	*flhA*	Flagellar biosynthesis protein	−307.03
PMI1636	*fliL*	Flagellar protein FliL	−302.51
PMI1648	*flgH*	Flagellar L-ring protein precursor	−297.81
PMI1630	*fliF*	Flagellar M-ring protein	−286.30
PMI1638	*fliN*	Flagellar motor switch protein	−279.07
PMI1634	*fliJ*	Flagellar protein FliJ	−276.57
PMI1629	*fliE*	Flagellar hook-basal body complex protein	−261.77
PMI1623	*fliT*	Flagellar protein	−242.66
PMI1469	*fim8A*	Fimbrial subunit	−234.31
PMI3460		Putative lipoprotein	−227.61
PMI3115	*umoA*	Putative upregulator of flagellar operon	−222.72
PMI1633	*fliI*	Flagellum-specific ATP synthase	−192.53
PMI1669	*motB*	Chemotaxis protein (motility protein B)	−174.67
PMI1617	*fliZ*	FliZ protein	−161.68
PMI1655	*flgA*	Flagellar basal body P-ring formation protein	−152.90
PMI1640	*fliP*	Flagellar biosynthetic protein	−140.09
PMI1621	*flaD*; *fliD*	Flagellar hook-associated protein 2	−127.34
PMI1653	*flgC*	Flagellar basal body rod protein	−122.76
PMI1650	*flgF*	Flagellar basal body rod protein	−98.71
PMI0833		Putative exported protein	−95.10
PMI2421		Putative phospholipid-binding protein	−78.61
PMI0599	*modC*	Molybdenum ABC transporter, ATP-binding protein	−76.09
PMI1622	*fliS*	Flagellar protein FliS	−70.74
PMI0182		Putative transcriptional regulator (MrpJ homolog)	−70.05
PMI1656	*flgM*	Negative regulator of flagellin synthesis (anti-sigma-28 factor)	−66.60
PMI1668	*cheA*	Chemotaxis protein	−62.85
PMI1645	*flgK*	Flagellar hook-associated protein 1	−62.65
PMI1642	*fliR*	Flagellar biosynthetic protein	−62.63
PMI1649	*flgG*	Flagellar basal body rod protein (distal rod protein)	−61.59
PMI1540		Putative transcriptional regulator	−56.75
PMI1663	*cheB*	Chemotaxis response regulator protein-glutamate methylesterase	−53.46
PMI1646	*flgJ*	Peptidoglycan hydrolase (muramidase)	−46.92
PMI1651	*flgE*	Flagellar hook protein	−46.64
PMI1666	*cheD*	Methyl-accepting chemotaxis protein	−41.63
PMI2808		Methyl-accepting chemotaxis protein	−37.69
PMI1470	*fim8J*	Fimbrial operon regulator	−37.36
PMI1665	*tap*	Methyl-accepting chemotaxis protein	−35.58
PMI1664	*cheR*	Chemotaxis protein methyltransferase	−31.00

[a] ORF, open reading frame.

TABLE 2 Top 50 genes induced in *mrpJ* overexpression strain compared to vector control

ORF	Gene	Annotation[a]	Fold change
PMI0271	*mrpJ*	Fimbrial operon regulator	2,178.32
PMI0748		Type VI secretion system protein	23.45
PMI0747		Type VI secretion system protein	20.49
PMI0347	*lysA*	Diaminopimelate decarboxylase	15.29
PMI3238	*argB*	Acetylglutamate kinase	13.95
PMI0749		Type VI secretion system protein	12.81
PMI0263	*mrpA*	Major mannose-resistant/*Proteus*-like fimbrial protein	12.28
PMI2157	*fruK*	1-Phosphofructokinase	12.18
PMI1079		Conserved hypothetical protein	9.43
PMI1702		Putative membrane protein	8.92
PMI2292	*ptsG*	PTS system, glucose-specific IIBC component	8.70
PMI0287		Putative amidohydrolase/metallopeptidase	8.01
PMI2528	*hyfA*	Hydrogenase 4 component A	6.21
PMI2755	*lysC*	Lysine-sensitive aspartokinase III	5.68
PMI2307	*argA*	Amino acid acetyltransferase	5.22
PMI0744		Putative phosphopeptide-binding protein; type VI secretion	5.15
PMI0742		Type VI secretion system protein	5.12
PMI2660	*caiF*	Transcriptional activator for carnitine metabolism	4.93
PMI2825	*def*	Peptide deformylase	4.92
PMI0746		Type VI secretion system protein	4.84
PMI2523	*hyfF*	Hydrogenase 4 component F	4.66
PMI3577	*fdhF*	Formate dehydrogenase H, selenopolypeptide subunit	4.30
PMI0741		Type VI secretion system protein	4.18
PMI2821	*argD*	Acetylornithine/succinyldiaminopimelate aminotransferase	3.87
PMI1777		PTS system IIA component	3.60
PMI2873		Putative acetyltransferase	3.56
PMI0667		Putative exported protein	3.31
PMI3225		Putative membrane protein	3.19
PMI3581	*hydN*	Electron transport protein	3.17
PMI3457	*argI*	Ornithine carbamoyltransferase chain I	3.12
PMI3553	*trkH*	Trk system potassium uptake protein	3.12
PMI2769	*purD*	Phosphoribosylamine-glycine ligase	3.01
PMI3125	*hipA*	Putative regulatory protein	3.00
PMI2288	*dapD*	2,3,4,5-Tetrahydropyridine-2-carboxylate *N*-succinyltransferase	2.96
PMI2661	*fsaA*	Fructose-6-phosphate aldolase	2.90
PMI0637	*moeA*	Molybdopterin biosynthesis protein	2.82
PMI1263		Putative membrane protein	2.82
PMI0967		Phage protein	2.66
PMI0030	*exbD*	Biopolymer transport protein	2.57
PMI2956	*chbB; celA*	*N*,*N*′-diacetylchitobiose-specific PTS system, EIIb component	2.55
PMI0244		Putative membrane protein	2.53
PMI3698		Putative membrane protein	2.44
PMI2761	*eda*	KHG/KDPG aldolase	2.39
PMI1023		Putative kinase	2.33
PMI0825	*ndpA*	Nucleoid-asociated protein	2.33
PMI1313	*pyrF*	Orotidine-5′-phosphate decarboxylase	2.32
PMI3141		Putative restriction endonuclease	2.29
PMI2360		Adenylate cyclase-like protein	2.29
PMI2168		Probable short-chain dehydrogenase	2.27
PMI1405	*pykF*	Pyruvate kinase	2.27

[a] PTS, phosphotransferase; KHG, 2-keto-4-hydroxyglutarate; KDPG, 2-keto-3-deoxy-6-phosphogluconate.

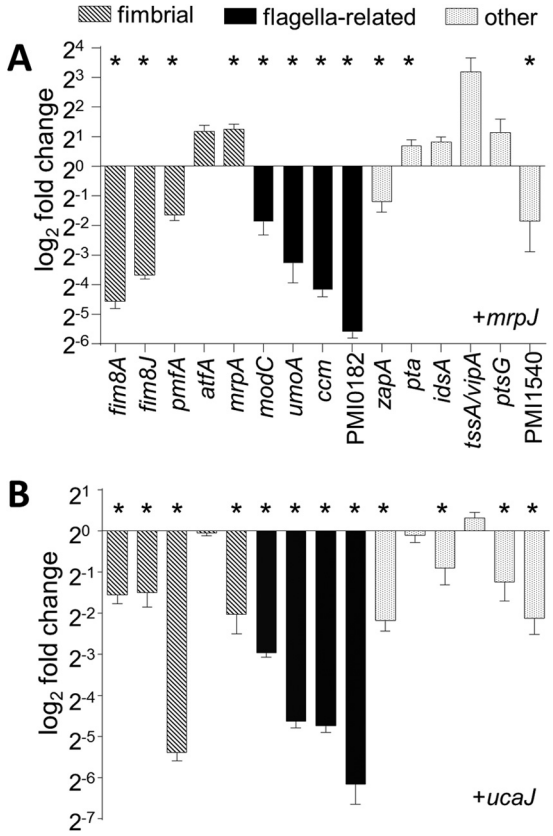

FIG 2 qRT-PCR validation of selected microarray data. (A) Gene expression by the *mrpJ in vivo* mimic strain compared to the vector control. (B) Gene expression by a *ucaJ* overexpression strain. Data are the results of three independent experiments, normalized to *rpoA*, and error bars show standard errors of the means (SEM). Statistically significant differences compared to vector control ($P < 0.05$) as calculated by Student's unpaired *t* test are indicated by an asterisk.

mental material). Even though the observed fold changes in the Δ*mrpJ* mutant were very modest, gene expression was generally the inverse of the *in vivo* mimic strain. For example, *mrpA* was induced by *mrpJ*, and flagellum- or swarming-related genes were repressed, while in the Δ*mrpJ* strain, transcript levels of *mrpA* were downregulated and those of motility-associated genes increased. Of the 15 *mrpJ* paralogs encoded by *P. mirabilis* genes, *ucaJ* is among the strongest in its repression of motility (33); therefore, we also tested the effect of *ucaJ* overexpression on *mrpJ*-regulated genes (Fig. 2B). As expected, flagellum-related genes were approximately 2-fold more repressed by *ucaJ* than by *mrpJ*. Interestingly, *ucaJ* did not induce the T6SS, and regulation of fimbrial and other virulence-associated genes varied in both direction and magnitude compared to that of *mrpJ*.

Promoter deletion analysis identifies an MrpJ-responsive region in the *mrpA* promoter. Following our transcriptomic identification of *mrpJ* targets, we sought to deepen our mechanistic understanding of transcriptional regulation by MrpJ. To start to address this question, we determined the promoter fragment required for *mrpJ*-dependent induction of the *mrp* operon. Expression of MR/P fimbriae is phase variable in response to environmental stimuli by means of an invertible element (23, 63) (Fig. 3A). 5′ RACE mapped the transcriptional start of *mrpA* to the

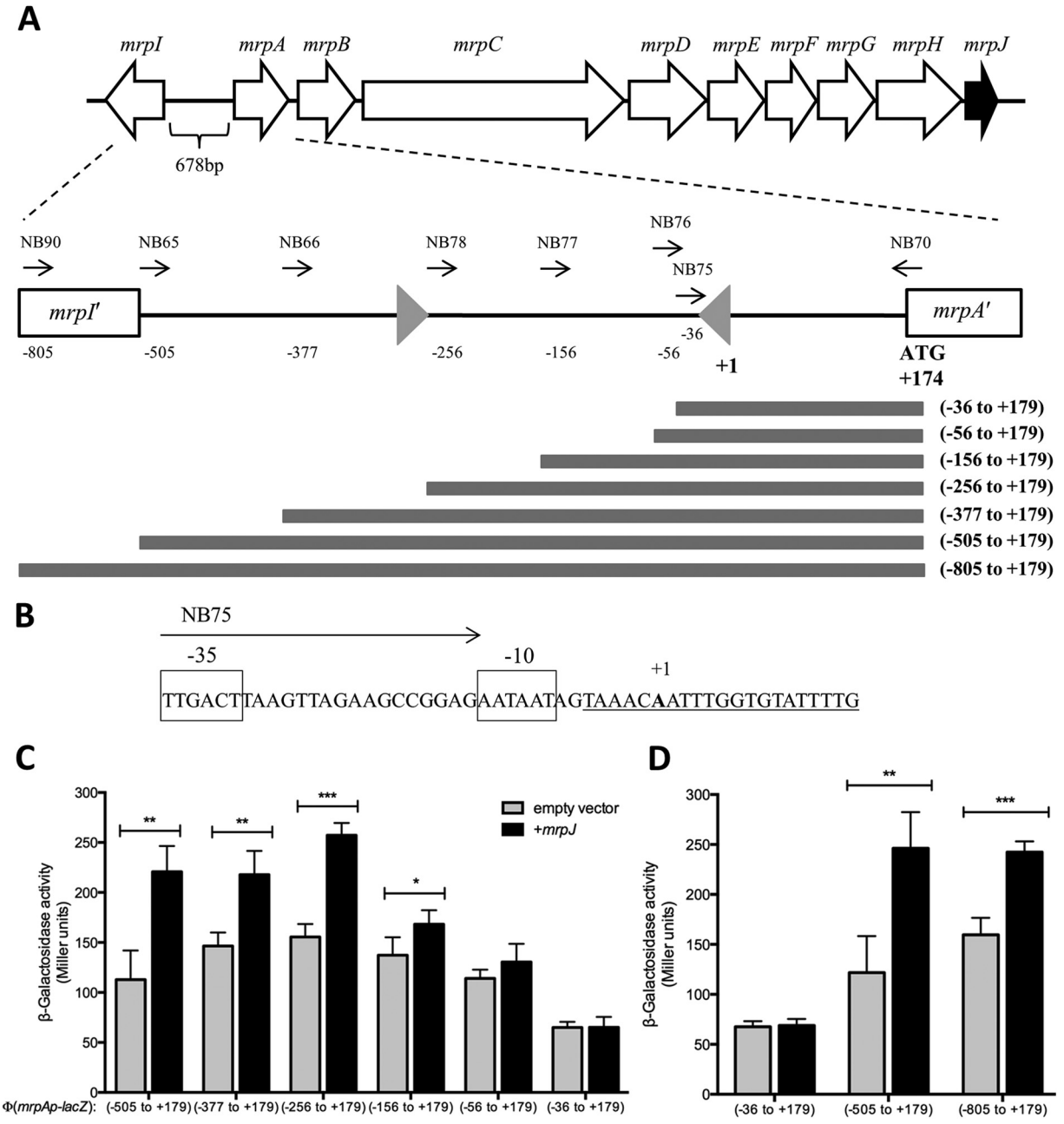

FIG 3 MrpJ-dependent activation of Φ(*mrpAp-lacZ*) expression. (A) Schematic showing the *mrp* gene locus, including *mrpI* and the fimbrial operon *mrpABCDEFGHJ*. The intergenic region contains an invertible element flanked by inverted repeats (gray triangles) here depicted in the ON orientation, resulting in MR/P fimbria production. The numbers are the 5′ positions of Φ(*mrpAp-lacZ*) operon fusions relative to the transcriptional start site of *mrpA* (+1), which was determined by 5′ RACE. Gray bars visualize Φ(*mrpAp-lacZ*) operon fusions with respect to the included promoter elements. (B) Nucleotide sequence surrounding the transcriptional start site of *mrpA*. The inverted repeat sequence is underlined; the transcriptional start site (+1) is indicated by bold type. Putative −10 and −35 regions are boxed and labeled. (C and D) Effect of promoter truncation on *mrpJ*-dependent activation of Φ(*mrpAp-lacZ*) expression in mid-logarithmic growth phase. Single-copy fusions to *lacZ* include specified amounts of DNA upstream of the predicted MrpA start codon. Strains were transformed with empty vector (pLX3607) or *mrpJ* expression plasmid (pLX3805; black bars). β-Galactosidase activity was determined as described in Materials and Methods. Values represent the means of four independent experiments plus standard deviations (SD) (error bars). Statistically significant differences comparing presence or absence of *mrpJ* as calculated by Student's unpaired *t* test are indicated by bars and asterisks as follows: *, $P \leq 0.05$; **, $P \leq 0.01$; ***, $P \leq 0.001$.

adenine residue located 173 residues upstream of the predicted ATG start codon. This residue is located within the inverted repeat closest to *mrpA*. Visual inspection of the sequence immediately upstream of the start of transcription revealed the presence of putative −10 and −35 regions separated by a 17-bp spacer, both of which closely match the consensus sequence of a bacterial σ^{70} promoter (64) (Fig. 3B), when the invertible element is in the ON position, allowing transcription of the *mrp* operon. Of note, a

previously reported canonical σ^{70} promoter sequence facing *mrpA* in the ON orientation (23) could not be located on the sequenced genome of strain HI4320.

To identify the promoter region necessary for MrpJ-dependent activation of *mrpA* expression, we constructed a set of single-copy Φ(*mrpA-lacZ*) operon fusion strains. All *lacZ* fusion strains contained different lengths of DNA upstream of *mrpA* (Fig. 3A) integrated at the *att*Tn*7* chromosomal locus downstream of *glmS*. The reverse primer was chosen to anneal to the beginning of the *mrpA* coding sequence to ensure all relevant regulatory elements are included in our transcriptional fusions. During aerobic growth, *P. mirabilis* exists as a mixed population of bacteria expressing MR/P fimbriae (promoter in the ON position) and those that do not (invertible element OFF). To avoid complication of our results by variation of *mrpJ* expression from its native promoter, we utilized a previously described insertion-disruption mutant in *mrpI* (32), which has the invertible element in the OFF orientation (L-OFF). MrpI is the only recombinase known to control phase variation of MR/P fimbriae (20). Hence, this mutation irreversibly locks the invertible element in the OFF position, thereby eliminating production of MR/P fimbriae. All strains were cultured to replicate the experimental conditions of the transcriptomic analysis.

An operon fusion comprising the whole intergenic region of *mrpI* and *mrpA* to *lacZ* (nucleotides −505 to +179) responded to *mrpJ* expression in *trans*, with β-galactosidase levels increasing approximately 2-fold compared to an empty vector control (Fig. 3C). Activities of two other constructs containing shorter fragments of the intergenic region (from −377 to +179 and from −256 to +179) showed induction levels similar to that of the full-length intergenic region, suggesting that these 249 bp do not contribute to MrpJ-dependent activation of Φ(*mrpAp-lacZ*) expression. The highest overall activity under Φ(*mrpAp-lacZ*)-inducing conditions (+*mrpJ*) was measured for the construct from −256 to +179. Induction of the construct from −156 to +179 by MrpJ was significantly reduced and completely abolished upon further deletion of an additional 100 nucleotides (−56 to +179). These results imply that the region between 256 and 156 bp upstream of the transcriptional start of *mrpA* is required for MrpJ-mediated induction of Φ(*mrpAp-lacZ*) expression. The small, albeit statistically significant, response to MrpJ production by the fragment from −156 to +179 may suggest the presence of a partial MrpJ binding site, although the biological significance of this result has yet to be established.

The shortest promoter fragment tested (nucleotides −36 to +179) showed low levels of β-galactosidase activity unaffected by *mrpJ* overexpression (Fig. 3C). This construct contains the predicted −35 and −10 region, resulting in basal expression of the Φ(*mrpAp-lacZ*) fusion. Including an additional 20 nucleotides upstream (−56 to +179) results in a marked increase in transcription independent of MrpJ production, demonstrating that MrpJ is most likely not the only factor activating *mrpA* transcription.

Validation of epitope-tagged MrpJ for use in ChIP assay. To further dissect mechanistic aspects of MrpJ-mediated transcriptional regulation, we performed ChIP analysis to define MrpJ-DNA interactions *in vivo* in the native state of the bacterial chromosome. In order to conduct these experiments, we validated an expression system that was compatible with ChIP. MrpJ with a C-terminal His_6 tag under the tight regulation of an arabinose-inducible promoter was expressed in *trans* (pMP190) in *P. mirabilis* HI4320 to match the *mrpJ* expression level to the *in vivo* level found during the course of UTIs in mice (24).

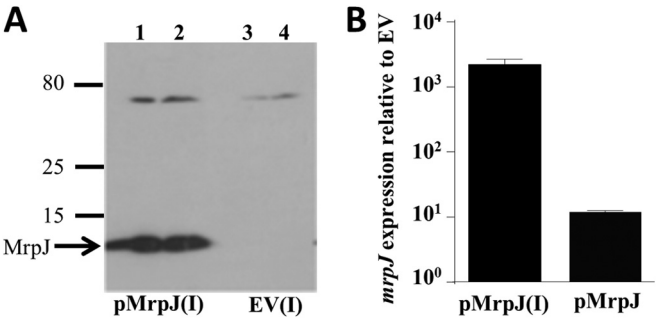

FIG 4 Validation of *mrpJ* expression system used in ChIP assay. (A) Levels of MrpJ analyzed by Western blotting. The gel was loaded with 5 μl (lanes 1 and 3) or 10 μl (lanes 2 and 4) of pMrpJ or empty vector (EV) lysate, respectively, induced (I) by 0.002% arabinose. The positions of size markers (in kilodaltons) are shown to the left of the gel. (B) *mrpJ* transcript level in the induced (I) or uninduced pMrpJ strain compared to EV by qRT-PCR; error bars indicate SEM of replicates, and data are from two independent experiments.

To confirm that the antibody for our ChIP assay recognized MrpJ protein without significant cross-reactivity, immunoblot analysis was performed on arabinose-induced pMP190 and vector control lysates harvested at an approximate OD_{600} of 2. As shown in Fig. 4A, probing of His_6-tagged MrpJ by this anti-His_5 antibody is highly specific. To verify even loading, samples were also separated on a parallel gel, and the proteins were visualized using Coomassie blue staining (see Fig. S2A in the supplemental material). Figure 4B shows the transcript level of *mrpJ* from pMP190 (pMrpJ) with or without arabinose induction. Quantitative RT-PCR was performed to measure *mrpJ* expression compared to the vector control at an OD_{600} of 2 (0.002% arabinose induction at an OD_{600} of 0.5), normalized to the level of *rpoA*. The induced sample [pMrpJ(I)] had 2,251-fold-more expression of *mrpJ* compared to the uninduced sample, similar to the level found during the progression of murine UTI (1 day postinfection, 1,103-fold induced over *in vitro* control [24]).

No significant difference in the growth pattern was found when growth curve analysis of *P. mirabilis* HI4320/pMP190 (pMrpJ) and the vector control (empty vector) with and without an arabinose induction (0.002%) was performed (see Fig. S2B and S2D in the supplemental material). Both strains were subcultured in 1:100 dilutions from an overnight aerated culture and allowed to reach stationary phase, a native state for *mrp* fimbrial operon induction (17). Serial dilution of this culture (OD_{600} of 2) resulted in no obvious distinction in CFU.

The length of the sonicated fragment of the cross-linked protein-DNA complexes is a major determinant of a successful ChIP experiment (65). For this study, we sheared the formaldehyde-cross-linked MrpJ-DNA complexes into a final range of 200- to 650-bp fragments as shown in the representative sonication profile in Fig. S2C in the supplemental material.

ChIP shows *in vivo* binding of the *mrp* promoter by MrpJ. An approximately 2-kb region upstream from the translational start site of *mrpA* was analyzed for *in vivo* MrpJ binding by ChIP-PCR. Figure 5A shows a schematic organization of this upstream regulatory sequence, including the invertible element (IE) region and the *mrpI* gene required for ON/OFF switching of the promoter orientation. The entire region, starting with *mrpA* and going up to

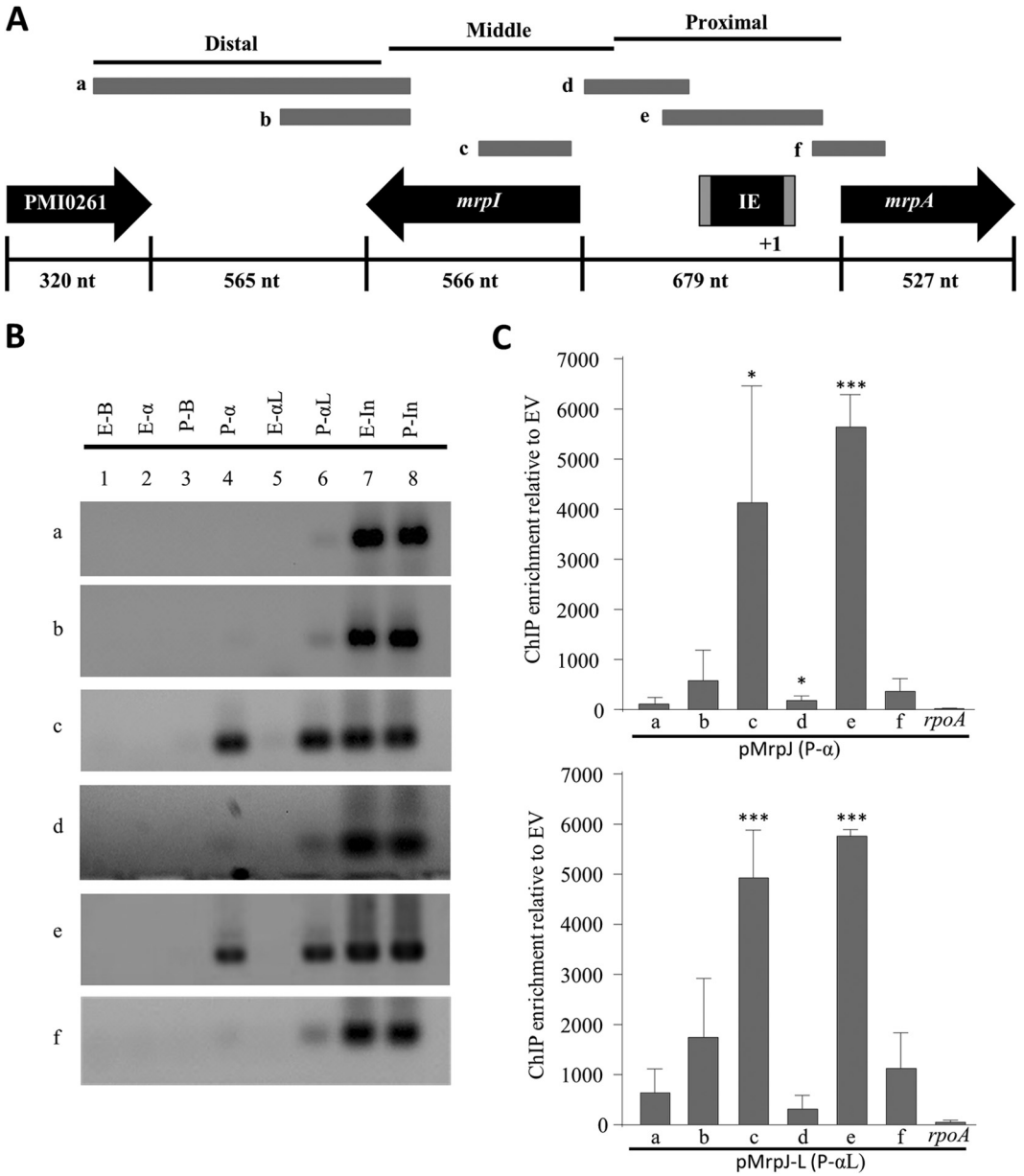

FIG 5 ChIP-PCR analysis of *mrpA* upstream promoter element. (A) Schematic representation of *mrpA* genomic organization depicting fragments "a" to "f" tested by ChIP-PCR as gray bars. The invertible element (IE) is not drawn to scale. nt, nucleotides. (B) Agarose gel analysis of *mrpA* ChIP-PCR. Lanes 1 to 8 are as follows: E-B, empty vector bead control; E-α, empty vector His_5-IP; P-B, MrpJ plasmid bead control; P-α, MrpJ plasmid His_5-IP with antibody-coupled beads; E-αL, empty vector His_5-IP using antibody-coupled lysate; P-αL, MrpJ plasmid His_5-IP using antibody-coupled lysate; E-In, 10% pre-IP empty vector input; P-In, 10% pre-IP MrpJ plasmid input. The results of one experiment are shown. We performed three experiments with similar results. (C) Image Studio analysis of ChIP-PCR data. MrpJ-His_6 ChIP signal enrichment is shown relative to the EV signal (comparing data from panel B [lanes 4 versus 2 or lanes 6 versus 5]). The means of three independent ChIP experiments are shown in the graphs; error bars represent standard deviations. Statistically significant differences compared to the *rpoA* enrichment value as calculated by Student's unpaired *t* test are indicated by asterisks as follows: *, $P \leq 0.05$; ***, $P \leq 0.001$.

PMI0261, has been divided into base pair length landmarks for easy reference. A series of primers was designed to walk toward the translational start of *mrpA* in graduated steps of PCR amplicons. Amplified fragments were designated as proximal, middle, and distal based on their relative proximity to the start site. Figure 5B shows the results for one representative ChIP-PCR gel analysis, and Fig. 5C shows the average values from three independent experiments for the *mrp* promoter.

Two primer sets were used to probe for the distal 5′ element relative to the start site; of these, the set encompassing the larger amplicon, fragment "a" (661 bp), showed little signal in all three of our ChIP assays (Fig. 5B and C). The ChIP signal increased slightly with the shorter amplicon, fragment "b" (443 bp), which had the forward primer nested 195 bp downstream, indicating a potential direct binding of MrpJ in the vicinity. Indeed, as we PCR walked into the *mrpI* intragenic region with fragment "c" (250 bp), the ChIP signal became highly pronounced, confirming *in vivo* MrpJ-DNA complex formation in this site. The approximate total length

of the area flanked by fragments "b" and "c" (with a 236-bp gap in between) is about 929 bp. On the basis of our 200- to 650-bp sonicated DNA fragment range in each ChIP experiment, we believe that the gradually increasing ChIP signals from fragments "b" to "c" stem from a single MrpJ nucleoprotein complex and that the minor residual population of larger sonicated fragments, as shown in Fig. S2C in the supplemental material, could account for the slight IP signal for fragment "b." ChIP signal was completely lost as we PCR walked further into the *mrpI* proximal putative promoter region, as shown by fragment "d," further supporting the specificity of MrpJ-DNA complex formation in the *mrpI* intragenic region.

The 679-bp intergenic region between *mrpI* and *mrpA* contains the invertible element. As described earlier, our β-galactosidase reporter assays have shown a consistently strong transcriptional activation of *mrpA* with the construct from nucleotides −256 to +179 and longer promoter elements (Fig. 3), which include the IE region in its ON orientation. We extended our ChIP-PCR walk into the proximal promoter region of *mrpA* with fragment "e" (300 bp), which encases the IE and its flanking inverted repeat sequences. Consistent with the reporter assay data, we found the strongest *in vivo* MrpJ binding in this region, suggesting that the MrpJ-dependent activation of *mrpA* in the transcriptional reporter strains is a direct result of nucleoprotein complex formation and feedback regulation by MrpJ on this site. ChIP signal was lost as we PCR walked further downstream of the intergenic region between *mrpI* and *mrpA* and with the inclusion of *mrpA* intragenic sequence fragment "f" (199 bp). Robust PCR amplicons in the input samples showed that the low or negligible ChIP-PCR signal with some of our primer sets is not due to inefficient PCRs; rather, they support the specificity of the positive ChIP signals.

Our data suggest that MrpJ directly autoregulates the *mrp* operon *in vivo* and that there are two direct MrpJ interaction regions on the *mrpA* promoter; the distal site is located in the intragenic region of *mrpI*, and the proximal one is located within the invertible element. To test whether the *mrpI* site contributes to MrpJ regulation of *mrpA*, we examined this new site using the transcriptional reporter assay; including the distal binding site within *mrpI* (−805 to +179) did not further increase MrpJ-dependent expression of Φ(*mrpAp-lacZ*) (Fig. 3D). Indeed, the fold change measured for the promoter fragment including *mrpI* was almost identical to that observed for the transcriptional fusion restricted to the full intragenic region between *mrpI* and *mrpA*.

ChIP demonstrates *in vivo* MrpJ-DNA complex formation on the *flhDC* promoter. Next, we extended our ChIP-PCR analysis to the *flhDC* upstream promoter element, an operon previously shown to be repressed by MrpJ (32, 33). Figure 6A shows a schematic diagram of the genomic organization of this region, specifically depicting the regions amplified for our analysis. The transcriptional start we identified for *flhD* by 5′ RACE is in agreement with an earlier reported putative start site in another strain of *P. mirabilis* (66). The most distal fragment, fragment "g" (373 bp), showed positive MrpJ binding signal, especially in the antibody-coupled lysate IP for anti-His_5-MrpJ. While first conjugating the antibody with the beads prior to the addition of lysate (P-α) could yield lower IP background, coupling the lysate with antibody before bead addition (P-αL) augments signal enrichment. We found that immunoprecipitation of MrpJ-His_6 using antibody-coupled lysate (P-αL) provided greater efficiency than IP of MrpJ-His_6 using antibody-coupled beads. The ChIP signal was reproducibly lost when we PCR walked further downstream (fragment "h" [322 bp]) into the middle section but started to enhance with the mid-proximal transition amplicon, fragment "i" (241 bp). The signal was further pronounced with the proximal "j" fragment (356 bp), corresponding to the previously reported EMSA probe for MrpJ binding *in vitro*. Based on our 5′ RACE data, this region also carries the transcriptional start site; this set was used as a positive control in all of our ChIP assays. The length of DNA flanked by fragments "i" and "j" is 597 bp. On the basis of the sonication fragment range maintained in our ChIP assays (200 to 650 bp), we believe the gradual increase in binding signal from these two sets (fragments "i" and "j") originates from one MrpJ binding event. To our surprise, a fragment primarily within *flhD* coding sequence (fragment "k" [283 bp]) placed 183 bp downstream of fragment "j" provided a very strong positive ChIP signal in all three of our independent experiments. This was intriguing to us, as based on the earlier *in vitro* EMSA data, we did not expect to see *flhD* intragenic MrpJ binding signal. Although the total linear length of DNA encompassing fragments "j" and "k" is 822 bp, larger than the size range of our sonication fragments (200 to 650 bp), a slim chance remains for intermediate length fragments carrying the "k" amplicon on their 3′ end and the MrpJ binding region on their 5′ side. It is also possible that MrpJ forms more than one viable nucleoprotein complex on the proximal and internal regions of *flhDC*. To evaluate whether this is occurring, *flhC* intragenic PCR was performed, and a strong ChIP signal was found in that region as well (fragment "l"). The proximal promoter region and the *flhD* gene are potentially part of a more complex conformation than their usually perceived linear structure. This would give rise to a comparatively condensed DNA before cross-linking and sonication, generating a much longer DNA fragment after the reversal of cross-linking even if only one DNA-protein interaction had happened *in vivo* (67–70).

MrpJ modulates *P. mirabilis* pathogenesis in an *in vivo* mouse UTI model. Previously, an *mrpJ* mutant was found to be outcompeted by wild-type strain HI4320 in a mouse coinfection UTI model (32). Our transcriptional analyses showed a diverse virulence gene network under MrpJ, expanding its contribution beyond flagellar and *mrp* fimbrial regulation. Genes modulating such a broad virulence network may have a greater effect on a pathogen's fitness, and we hypothesized that deletion of *mrpJ* would lead to a profound decrease in virulence even when the mutant was not in direct competition with the wild-type parent strain. Hence, to address whether *mrpJ* deficiency can directly affect *P. mirabilis* virulence within the urinary tract, we challenged mice with monocultures of *P. mirabilis* isolate HI4320 or the isogenic Δ*mrpJ* mutant using a murine UTI model. As shown in Fig. 7, bladder colonization was highly compromised in the absence of functional MrpJ (approximately 10,000-fold; $P = 0.0079$), whereas kidney samples show a comparatively moderate effect. As previously reported (32), there was no significant deviation in the *in vitro* growth profile comparison between the *mrpJ* mutant and wild-type HI4320, indicating that MrpJ is involved in the regulation of the *P. mirabilis* pathogenic lifestyle in the lower urinary tract.

DISCUSSION

The inverse interplay between fimbria-mediated attachment and flagellar motility in *P. mirabilis* is critical for the establishment of a successful infection in the urinary tract (5). Earlier studies have shown that MrpJ plays an important role in this dynamic by pos-

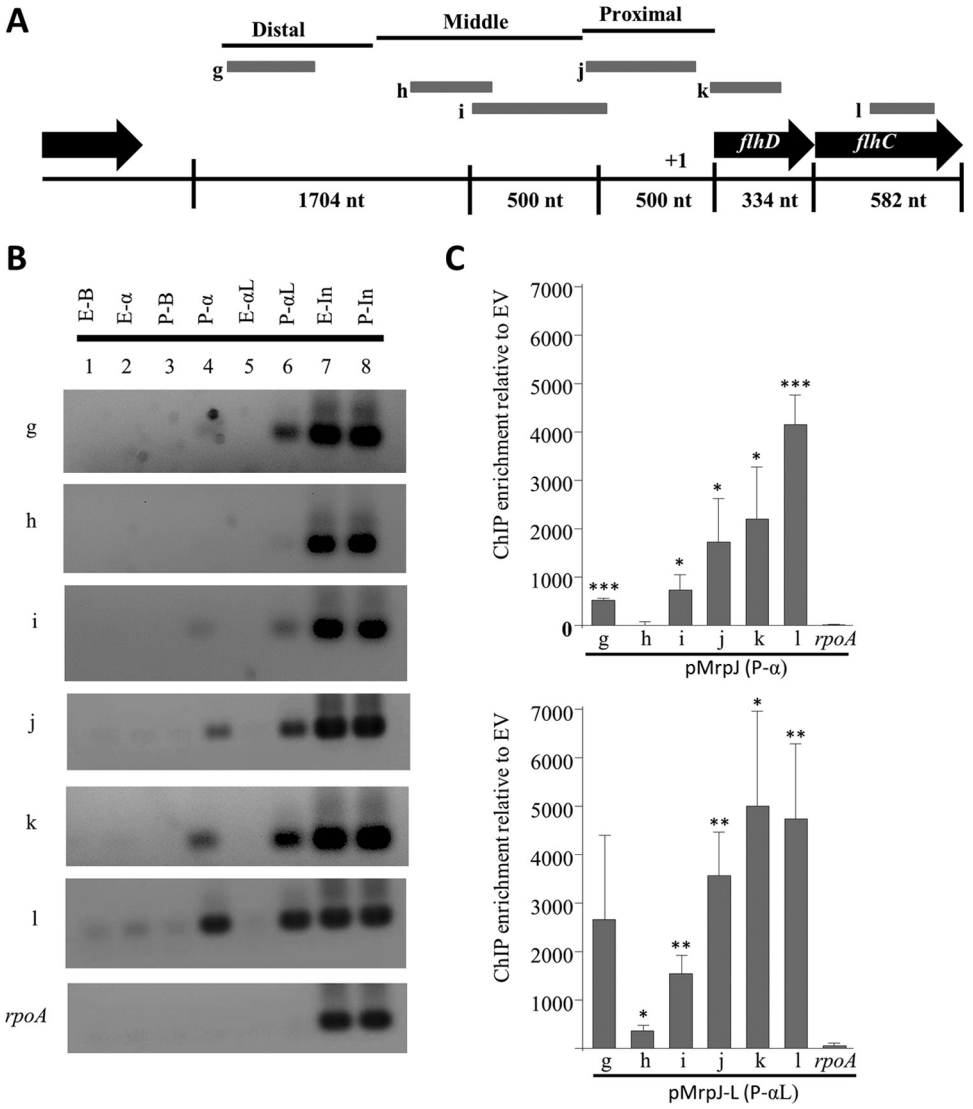

FIG 6 ChIP-PCR analysis of *flhDC* upstream promoter element and intragenic region. (A) Schematic representation of *flhDC* genomic organization depicting the fragments "g" to "l" tested by ChIP-PCR as gray bars. (B) Agarose gel analysis of *flhDC* ChIP-PCR. Lane designations are the same as in Fig. 5B. The results of one representative experiment are shown (three experiments were performed). (C) Image Studio analysis of *flhDC* ChIP-PCR data. MrpJ-His_6 ChIP signal enrichment is shown relative to the EV signal. The averages of three independent ChIP experiments are shown; error bars represent standard deviation. Statistically significant differences compared to the *rpoA* enrichment value as calculated by Student's unpaired *t* test are indicated by asterisks as follows: *, $P \leq 0.05$; **, $P \leq 0.01$; ***, $P \leq 0.001$.

itively regulating its own operon while repressing flagella through the flagellar master regulator *flhDC* (32, 33). The present study expands the role of MrpJ beyond this interplay by identifying an array of cellular processes and target genes under its influence, showing a more global regulation of virulence by this transcriptional modulator. On the basis of our microarray and qRT-PCR data, we propose that MrpJ is a master regulator of *P. mirabilis* virulence (Fig. 8).

P. mirabilis HI4320 encodes 15 *mrpJ*-type genes (33), and most of these also act to repress motility. All but four are located within fimbrial operons. We propose that MrpJ is the dominant regulator of this network during UTIs. First, the highest levels of *mrpJ* transcript are detected in urine samples from infected mice, and the *mrp* operon is the most highly induced set of genes during the shift from *in vitro* to *in vivo* growth (24). Second, 13/14 of the other *mrpJ* paralogs are expressed during infection at or below background detection levels (24); the exception is orphan gene PMI0982 which although detectable, is not differentially expressed *in vivo*. Third, the data we present demonstrate that MrpJ controls numerous virulence processes, although this may occur via intermediate factors, as microarrays cannot discriminate between indirect and direct regulation. Fourth, MrpJ regulates other fimbrial operons, including *fim8* and *fim14*, both of which encode *mrpJ* paralogs. Indeed, *fim8J* was repressed by MrpJ in our microarray analysis. The aerated broth growth condition, while beneficial for detecting regulation of flagella, is not ideal for fimbrial expression, and it is possible that MrpJ regulates additional fimbriae that were not detected in this set of microarrays. Nevertheless, we performed our analysis using mid-logarithmic-phase cultures, which allowed us to carefully adjust *mrpJ* expression to

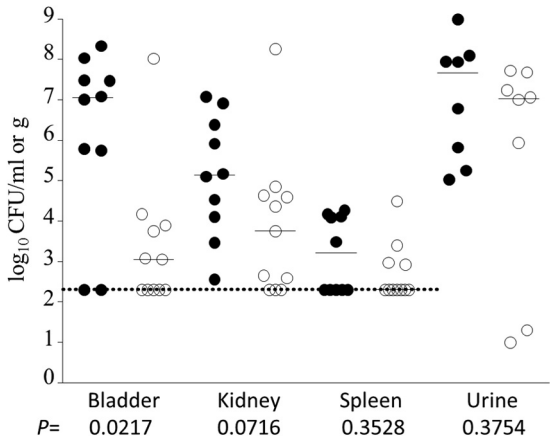

FIG 7 *P. mirabilis* HI4320Δ*mrpJ* challenge in a mouse model of ascending UTI. Deficiency of *mrpJ* compromises *P. mirabilis* fitness within the bladder. Female mice were infected via transurethral catheterization with either wild-type HI4320 or an isogenic *mrpJ* mutant in an independent challenge experiment. Each symbol represents the bacterial titer present in the bladder, kidney, spleen, or urine of an individual mouse at 7 days postinoculation. Bars denote median values for each group of mice (wild type [●] and mutant [○]). The dotted line indicates the limit of detection for homogenized organ data. Statistical significance was determined using the Mann-Whitney U test. Data depicted here are from two independent experiments.

mimic the amount that occurs during UTI. Last, two of the four orphan *mrpJ* paralogs, PMI0182 and PMI3508, were repressed by MrpJ. However, an important question remains: do other MrpJ paralogs contribute to virulence? It is possible that low levels of transcription of one or more *mrpJ* paralogs could trigger a regulatory cascade. Expression in *trans* of other *mrpJ* paralogs leads to differing surface fimbrial appearances (33), and we now show that *ucaJ* represses *mrpA*; it will be important to decipher the complete regulatory networks of UcaJ and other MrpJ paralogs to fully understand how *P. mirabilis* coordinates the expression of fimbria-encoding genes. It is possible that these related genes orchestrate genetic programs beneficial to specific niches beyond the bladder.

The sequencing and annotation of prototypic *P. mirabilis* strain HI4320 (8) revealed the presence of 17 different potential chaperone-usher fimbriae in its genome. Our microarray analysis has now shown that a number of these fimbriae are under the control of MrpJ; while MrpJ augmented *mrp* gene expression, *pmfA*, *fim8A*, and *fim14A* were downregulated. Interestingly, *pmfA* and *fim8A* were also repressed when gene expression was monitored in mice infected with strain HI4320 (24). Fimbrial regulation is a quintessential aspect of virulence in many pathogens, including causative agents of UTIs, and in many instances, more than one fimbrial type contributes to disease progression depending on the environmental cues or tissue niches (4, 71). Although several fimbriae, including MR/P, PMF, and Fim14, have been reported to modulate *P. mirabilis* pathogenesis, little is known about the regulation and combinatorial implication of fimbriae in *P. mirabilis*-mediated UTIs (13, 15, 57, 72). To our knowledge, this is the first report describing a molecular regulator simultaneously targeting a number of fimbriae in a positive or negative manner in this uropathogen.

Among other differentially regulated targets, we identified flagellum-related genes, including the flagellar master transcriptional regulator *flhDC* as anticipated based on the previously reported inverse play between MR/P and flagella (32, 33). Our microarray data show that MrpJ not only regulates flagella but also regulates factors specifically involved in swarming which are

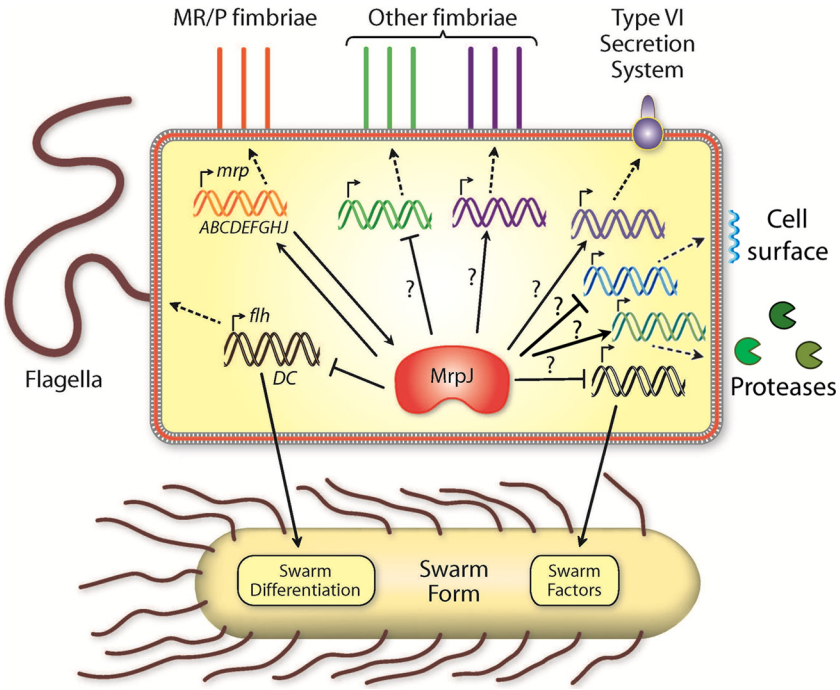

FIG 8 Model for MrpJ as a master regulator of virulence. MrpJ directly represses *flhDC* and induces the *mrp* operon. Other fimbriae (e.g., PMF, Fim8), the T6SS, cell surface modification systems (e.g., PagP, WzyE), and proteases (e.g., ZapA, Pta) are regulated by MrpJ, but this could be direct or indirect (represented by a question mark).

not necessarily under the control of $FlhD_4C_2$. These genes include the swarming regulator genes *umoA* and *umoB* (53), as well as *mrpJ* paralogs, which are not associated with fimbrial operons (PMI0182 and PMI3508) (33).

A number of T6SS genes were also induced by MrpJ; among them were the effector genes *idsADE* as well as seven T6SS structural genes. Although T6SS is involved in virulence in a variety of pathogens (5, 73–75), its role in UTIs has not yet been investigated. Recent reports have described the role of the *P. mirabilis* T6SS in the competition of some strains over others (60, 62), particularly when distinct isolates encounter each other while swarming. However, during *in vitro* swarming, the *mrp* operon is repressed (44). We speculate that the T6SS may play a swarming-independent role during infection by mediating direct interaction with the host, perhaps mediated by secretion of a different set of effector proteins. It is also possible that MrpJ-mediated regulation of T6SS components facilitates *P. mirabilis* swarming behavior across catheter surfaces in a polymicrobial environment when signals from the host are encountered.

In addition to these factors, several other putative or known virulence genes were revealed as the targets of MrpJ; the Pta toxin and ZapA metalloprotease have already been shown to contribute to UTI in mice (58, 76, 77). MrpJ regulates expression or modification of cell surface molecules, such as lipoproteins and LPS, which have been associated with virulence by other bacterial pathogens (78–81), and we hypothesize these changes aid *P. mirabilis* survival in the urinary tract by bolstering bacterial defenses against the innate immune response.

We chose two candidate virulence operons to perform further molecular analyses of MrpJ-mediated transcriptional regulation: *mrpABCDEFGHJ* and *flhDC*, an activation and a repression target, respectively. We used two molecular approaches to probe the nature of the MrpJ-target gene interactions: β-galactosidase reporter assays to determine the essential promoter element and ChIP analysis to evaluate the *in vivo* MrpJ-chromosome interaction. Our single-copy chromosomal operon fusions identified the necessary promoter region on the *mrpA* upstream element (Fig. 3C). Specifically, the highest LacZ activity was seen by the promoter fragment from nucleotides −256 to +179, which includes the invertible element region (Fig. 3C), and this was consistent with our *in vivo* ChIP data showing direct MrpJ binding in this region (fragment "e" [Fig. 5]). Interestingly, there was a mild decrease in LacZ activity with the longer promoter fragments used in this assay, indicating possible repressor binding. ChIP data further support this hypothesis, as there was only a background level of MrpJ binding in this region (fragment "d"). Intriguingly, ChIP also showed a second MrpJ-DNA interaction upstream of the *mrpA* regulatory element in the intragenic region of *mrpI*. However, because the distal site did not contribute to transcriptional activity of our reporter constructs, we believe that proximity of MrpJ to this upstream region is influenced by the curvature and conformation of DNA in this area of the native chromosome. A previous report showed that mutation of *mrpJ* leads to the *mrp* promoter invertible element being predominantly in the OFF orientation (63). Our data suggest this could be due to either MrpJ interaction with the invertible element or the *mrpI* coding sequence. It remains to be determined whether MrpJ binding to the *mrp* promoter affects transcription of *mrpI in vivo*.

The presence of an upstream regulatory region in conjunction with a more proximally situated (relative to the transcriptional start site) regulatory element is seen in many instances in bacteria (69, 82), and in the case of the *mrp* promoter, it would provide for an elegant mechanism of regulation between the recombinase MrpI and its target operon *mrp*. This is especially important for genes involved in virulence, such as *mrpA*, to exert more stringent control over transcriptional regulation depending on various environmental cues. Although our transcriptional reporters reaffirm the notion of MrpJ-mediated autoregulation of the *mrp* operon, we point out that the fold changes observed in the transcriptional reporter assays are smaller than those reported for our microarray data (Fig. 3; see Tables S3 and S4 in the supplemental material). We hypothesize that the combination of integrating the reporters at a nonnative chromosomal site, as well as the lower sensitivity of β-galactosidase assays compared to qRT-PCR measurements, contributed to this outcome.

Surprisingly, we detected a consistent intragenic ChIP signal in our assay of MrpJ-mediated *in vivo* regulation of *flhDC*. Internal binding of transcriptional regulators within a gene in bacteria has been seen in many instances, and recently, it has also been observed for *flhDC* and *fliA* (83–87). In this particular case of MrpJ-*flhDC* regulation, these intragenic signals could originate from additional MrpJ-DNA interactions, or alternatively, they could arise from a condensed higher-order conformation of the *P. mirabilis* chromosome in this region (67–70, 88). The intergenic region preceding the *flhDC* operon is quite large (over 2.7 kb) and highly AT rich (24.7% GC versus 38.9% chromosomal GC content) in this pathogen. Although we tested *flhD* transcriptional reporters with MrpJ, a significant reduction in *flhD* promoter activity was not seen reproducibly (data not shown). We hypothesize that a much larger upstream fragment in its native state is required to replicate MrpJ-mediated *flhD* promoter repression. To support the critical role of flagellar motility in various stages of this bacterium's life cycle, a number of regulators (e.g., H-NS, Crp, Lrp, RcsB, LrhA) have been shown or implicated to influence the *flhD* upstream region (5, 66, 89–91). Furthermore, it has recently been proposed that the *Salmonella enterica* global regulator LeuO binds to DNA differently to initiate or impede transcription of target genes (92). Distal as well as proximal binding profiles of MrpJ were evident for both the *mrp* gene and the *flhD* upstream regulatory element *in vivo*, suggesting that the binding of MrpJ on separate regions preceding its target genes occurs during both gene activation as well as repression. Therefore, our results warrant further studies to define the precise regulatory mechanism and structural reference of transcriptional regulation by MrpJ.

An obvious binding sequence for MrpJ could not be identified at this time. Although a repeat sequence was found in the MrpJ binding region of the *mrpA* promoter, this sequence was not found in the *flhDC* promoter. It is not uncommon for global bacterial transcriptional regulators to lack a consensus binding motif; in fact, a low level of binding specificity has been proposed as a genomic diagnostic tool to identify factors regulating genome-wide targets versus the local transcriptional regulators with highly specific binding sites (69, 70, 82, 93).

In *P. mirabilis*, this is the first report of a transcriptional modulator regulating a variety of processes, including several aspects of virulence. Our independent challenge experiments further highlight the critical role of MrpJ in virulence regulation in this bacterium. While the contribution of this regulator to UTI progression has been documented earlier in a cochallenge experiment in the presence of a wild-type counterpart (32), the direct modu-

latory effect of MrpJ deficiency is more evident in an individual challenge. However, the ability of this mutant to ascend to the kidney in spite of a poor bladder colonization profile implies that there could be other fimbriae compensating for the loss of MR/P fimbriae or perhaps involvement by other MrpJ paralogs.

In summary, this report analyzes the molecular nature of MrpJ-mediated transcriptional regulation in *P. mirabilis* by extending its contribution beyond the reciprocity of adherence and motility and introduces this regulator of transcription as a multifaceted virulence regulator of UTIs.

ACKNOWLEDGMENTS

We are grateful to Andrew Darwin for his input in the design of the β-galactosidase reporter assays, as well as his gift of the CC118 λ*pir* and pRS415 strains. We thank Herbert Schweizer for sending us plasmids pTNS3 and pUC18R6K-mini-Tn*7*T-Gm. We appreciate Jessica Schaffer and Keith Martinez for technical assistance with experiments and Gordon Cook for artwork. We also thank Aleksandra Sikora, Victor Torres, and Jessica Schaffer for critical reading of the manuscript.

This work was supported by U.S. Public Health Service grant AI083743 (M.M.P.) and in part by a grant from the Urology Care Foundation Research Scholars Program and AUA New York Section Research Scholar Fund (I.D.).

REFERENCES

1. **Hood MI, Skaar EP.** 2012. Nutritional immunity: transition metals at the pathogen-host interface. Nat Rev Microbiol **10:**525–537. http://dx.doi.org/10.1038/nrmicro2836.
2. **Troxell B, Hassan HM.** 2013. Transcriptional regulation by Ferric Uptake Regulator (Fur) in pathogenic bacteria. Front Cell Infect Microbiol **3:**59. http://dx.doi.org/10.3389/fcimb.2013.00059.
3. **Foxman B.** 2010. The epidemiology of urinary tract infection. Nat Rev Urol **7:**653–660. http://dx.doi.org/10.1038/nrurol.2010.190.
4. **Nielubowicz GR, Mobley HLT.** 2010. Host-pathogen interactions in urinary tract infection. Nat Rev Urol **7:**430–441. http://dx.doi.org/10.1038/nrurol.2010.101.
5. **Armbruster CE, Mobley HLT.** 2012. Merging mythology and morphology: the multifaceted lifestyle of *Proteus mirabilis*. Nat Rev Microbiol **10:**743–754. http://dx.doi.org/10.1038/nrmicro2890.
6. **Waksman G, Hultgren SJ.** 2009. Structural biology of the chaperone-usher pathway of pilus biogenesis. Nat Rev Microbiol **7:**765–774. http://dx.doi.org/10.1038/nrmicro2220.
7. **Lane MC, Alteri CJ, Smith SN, Mobley HLT.** 2007. Expression of flagella is coincident with uropathogenic *Escherichia coli* ascension to the upper urinary tract. Proc Natl Acad Sci U S A **104:**16669–16674. http://dx.doi.org/10.1073/pnas.0607898104.
8. **Pearson MM, Sebaihia M, Churcher C, Quail MA, Seshasayee AS, Luscombe NM, Abdellah Z, Arrosmith C, Atkin B, Chillingworth T, Hauser H, Jagels K, Moule S, Mungall K, Norbertczak H, Rabbinowitsch E, Walker D, Whithead S, Thomson NR, Rather PN, Parkhill J, Mobley HLT.** 2008. Complete genome sequence of uropathogenic *Proteus mirabilis*, a master of both adherence and motility. J Bacteriol **190:**4027–4037. http://dx.doi.org/10.1128/JB.01981-07.
9. **Adegbola RA, Old DC, Senior BW.** 1983. The adhesins and fimbriae of *Proteus mirabilis* strains associated with high and low affinity for the urinary tract. J Med Microbiol **16:**427–431. http://dx.doi.org/10.1099/00222615-16-4-427.
10. **Bahrani FK, Mobley HLT.** 1994. *Proteus mirabilis* MR/P fimbrial operon: genetic organization, nucleotide sequence, and conditions for expression. J Bacteriol **176:**3412–3419.
11. **Bijlsma IG, van Dijk L, Kusters JG, Gaastra W.** 1995. Nucleotide sequences of two fimbrial major subunit genes, *pmpA* and *ucaA*, from canine-uropathogenic *Proteus mirabilis* strains. Microbiology **141:**1349–1357. http://dx.doi.org/10.1099/13500872-141-6-1349.
12. **Cook SW, Mody N, Valle J, Hull R.** 1995. Molecular cloning of *Proteus mirabilis* uroepithelial cell adherence (*uca*) genes. Infect Immun **63:**2082–2086.
13. **Kuan L, Schaffer JN, Zouzias CD, Pearson MM.** 2014. Characterization of 17 chaperone-usher fimbriae encoded by *Proteus mirabilis* reveals strong conservation. J Med Microbiol **63:**911–922. http://dx.doi.org/10.1099/jmm.0.069971-0.
14. **Massad G, Bahrani FK, Mobley HLT.** 1994. *Proteus mirabilis* fimbriae: identification, isolation, and characterization of a new ambient-temperature fimbria. Infect Immun **62:**1989–1994.
15. **Massad G, Lockatell CV, Johnson DE, Mobley HLT.** 1994. *Proteus mirabilis* fimbriae: construction of an isogenic *pmfA* mutant and analysis of virulence in a CBA mouse model of ascending urinary tract infection. Infect Immun **62:**536–542.
16. **Wray SK, Hull SI, Cook RG, Barrish J, Hull RA.** 1986. Identification and characterization of a uroepithelial cell adhesin from a uropathogenic isolate of *Proteus mirabilis*. Infect Immun **54:**43–49.
17. **Bahrani FK, Massad G, Lockatell CV, Johnson DE, Russell RG, Warren JW, Mobley HLT.** 1994. Construction of an MR/P fimbrial mutant of *Proteus mirabilis*: role in virulence in a mouse model of ascending urinary tract infection. Infect Immun **62:**3363–3371.
18. **Jansen AM, Lockatell V, Johnson DE, Mobley HLT.** 2004. Mannose-resistant *Proteus*-like fimbriae are produced by most *Proteus mirabilis* strains infecting the urinary tract, dictate the in vivo localization of bacteria, and contribute to biofilm formation. Infect Immun **72:**7294–7305. http://dx.doi.org/10.1128/IAI.72.12.7294-7305.2004.
19. **Li X, Johnson DE, Mobley HLT.** 1999. Requirement of MrpH for mannose-resistant *Proteus*-like fimbria-mediated hemagglutination by *Proteus mirabilis*. Infect Immun **67:**2822–2833.
20. **Li X, Lockatell CV, Johnson DE, Mobley HLT.** 2002. Identification of MrpI as the sole recombinase that regulates the phase variation of MR/P fimbria, a bladder colonization factor of uropathogenic *Proteus mirabilis*. Mol Microbiol **45:**865–874. http://dx.doi.org/10.1046/j.1365-2958.2002.03067.x.
21. **Li X, Zhao H, Geymonat L, Bahrani F, Johnson DE, Mobley HLT.** 1997. *Proteus mirabilis* mannose-resistant, *Proteus*-like fimbriae: MrpG is located at the fimbrial tip and is required for fimbrial assembly. Infect Immun **65:**1327–1334.
22. **Zunino P, Sosa V, Schlapp G, Allen AG, Preston A, Maskell DJ.** 2007. Mannose-resistant *Proteus*-like and *P. mirabilis* fimbriae have specific and additive roles in *P. mirabilis* urinary tract infections. FEMS Immunol Med Microbiol **51:**125–133. http://dx.doi.org/10.1111/j.1574-695X.2007.00285.x..
23. **Zhao H, Li X, Johnson DE, Blomfield I, Mobley HLT.** 1997. *In vivo* phase variation of MR/P fimbrial gene expression in *Proteus mirabilis* infecting the urinary tract. Mol Microbiol **23:**1009–1019. http://dx.doi.org/10.1046/j.1365-2958.1997.2791645.x.
24. **Pearson MM, Yep A, Smith SN, Mobley HLT.** 2011. Transcriptome of *Proteus mirabilis* in the murine urinary tract: virulence and nitrogen assimilation gene expression. Infect Immun **79:**2619–2631. http://dx.doi.org/10.1128/IAI.05152-11.
25. **Li X, Erbe JL, Lockatell CV, Johnson DE, Jobling MG, Holmes RK, Mobley HLT.** 2004. Use of translational fusion of the MrpH fimbrial adhesin-binding domain with the cholera toxin A2 domain, coexpressed with the cholera toxin B subunit, as an intranasal vaccine to prevent experimental urinary tract infection by *Proteus mirabilis*. Infect Immun **72:**7306–7310. http://dx.doi.org/10.1128/IAI.72.12.7306-7310.2004.
26. **Li X, Lockatell CV, Johnson DE, Lane MC, Warren JW, Mobley HLT.** 2004. Development of an intranasal vaccine to prevent urinary tract infection by *Proteus mirabilis*. Infect Immun **72:**66–75. http://dx.doi.org/10.1128/IAI.72.1.66-75.2004.
27. **Pellegrino R, Galvalisi U, Scavone P, Sosa V, Zunino P.** 2003. Evaluation of *Proteus mirabilis* structural fimbrial proteins as antigens against urinary tract infections. FEMS Immunol Med Microbiol **36:**103–110. http://dx.doi.org/10.1016/S0928-8244(03)00103-2.
28. **Scavone P, Miyoshi A, Rial A, Chabalgoity A, Langella P, Azevedo V, Zunino P.** 2007. Intranasal immunisation with recombinant *Lactococcus lactis* displaying either anchored or secreted forms of *Proteus mirabilis* MrpA fimbrial protein confers specific immune response and induces a significant reduction of kidney bacterial colonisation in mice. Microbes Infect **9:**821–828. http://dx.doi.org/10.1016/j.micinf.2007.02.023.
29. **Scavone P, Rial A, Umpiérrez A, Chabalgoity A, Zunino P.** 2009. Effects of the administration of cholera toxin as a mucosal adjuvant on the immune and protective response induced by *Proteus mirabilis* MrpA fimbrial protein in the urinary tract. Microbiol Immunol **53:**233–240. http://dx.doi.org/10.1111/j.1348-0421.2009.00111.x.
30. **Scavone P, Sosa V, Pellegrino R, Galvalisi U, Zunino P.** 2004. Mucosal vaccination of mice with recombinant *Proteus mirabilis* structural fimbrial

proteins. Microbes Infect **6:**853–860. http://dx.doi.org/10.1016/j.micinf.2004.04.006.
31. **Scavone P, Umpiérrez A, Maskell DJ, Zunino P.** 2011. Nasal immunization with attenuated *Salmonella* Typhimurium expressing an MrpA-TetC fusion protein significantly reduces *Proteus mirabilis* colonization in the mouse urinary tract. J Med Microbiol **60:**899–904. http://dx.doi.org/10.1099/jmm.0.030460-0.
32. **Li X, Rasko DA, Lockatell CV, Johnson DE, Mobley HLT.** 2001. Repression of bacterial motility by a novel fimbrial gene product. EMBO J **20:**4854–4862. http://dx.doi.org/10.1093/emboj/20.17.4854.
33. **Pearson MM, Mobley HLT.** 2008. Repression of motility during fimbrial expression: identification of 14 *mrpJ* gene paralogues in *Proteus mirabilis*. Mol Microbiol **69:**548–558. http://dx.doi.org/10.1111/j.1365-2958.2008.06307.x.
34. **Reiss DJ, Mobley HLT.** 2011. Determination of target sequence bound by PapX, repressor of bacterial motility, in *flhD* promoter using systematic evolution of ligands by exponential enrichment (SELEX) and high throughput sequencing. J Biol Chem **286:**44726–44738. http://dx.doi.org/10.1074/jbc.M111.290684.
35. **Simms AN, Mobley HLT.** 2008. PapX, a P fimbrial operon-encoded inhibitor of motility in uropathogenic *Escherichia coli*. Infect Immun **76:**4833–4841. http://dx.doi.org/10.1128/IAI.00630-08.
36. **Allison SE, Silphaduang U, Mascarenhas M, Konczy P, Quan Q, Karmali M, Coombes BK.** 2012. Novel repressor of *Escherichia coli* O157:H7 motility encoded in the putative fimbrial cluster OI-1. J Bacteriol **194:**5343–5352. http://dx.doi.org/10.1128/JB.01025-12.
37. **Meslet-Cladiere LM, Pimenta A, Duchaud E, Holland IB, Blight MA.** 2004. In vivo expression of the mannose-resistant fimbriae of *Photorhabdus temperata* K122 during insect infection. J Bacteriol **186:**611–622. http://dx.doi.org/10.1128/JB.186.3.611-622.2004.
38. **He H, Snyder HA, Forst S.** 2004. Unique organization and regulation of the *mrx* fimbrial operon in *Xenorhabdus nematophila*. Microbiology **150:**1439–1446. http://dx.doi.org/10.1099/mic.0.26853-0.
39. **Altschul SF, Gish W, Miller W, Myers EW, Lipman DJ.** 1990. Basic local alignment search tool. J Mol Biol **215:**403–410. http://dx.doi.org/10.1016/S0022-2836(05)80360-2.
40. **Khalid MI, Teh LK, Lee LS, Zakaria ZA, Salleh MZ.** 2013. Genome sequence of *Proteus mirabilis* strain PR03, isolated from a local hospital in Malaysia. Genome Announc **1**(3)**:**e00327–13. http://dx.doi.org/10.1128/genomeA.00327-13.
41. **Minogue TD, Daligault HE, Davenport KW, Bishop-Lilly KA, Bruce DC, Chain PS, Coyne SR, Chertkov O, Freitas T, Frey KG, Jaissle J, Koroleva GI, Ladner JT, Palacios GF, Redden CL, Xu Y, Johnson SL.** 2014. Draft genome assemblies of *Proteus mirabilis* ATCC 7002 and *Proteus vulgaris* ATCC 49132. Genome Announc **2**(5)**:**e01064–14. http://dx.doi.org/10.1128/genomeA.01064-14.
42. **Shi X, Zhu Y, Li Y, Jiang M, Lin Y, Qiu Y, Chen Q, Yuan Y, Ni P, Hu Q, Huang S.** 2014. Genome sequence of *Proteus mirabilis* clinical isolate C05028. Genome Announc **2**(2)**:**e00167–14. http://dx.doi.org/10.1128/genomeA.00167-14.
43. **Sullivan NL, Septer AN, Fields AT, Wenren LM, Gibbs KA.** 2013. The complete genome sequence of *Proteus mirabilis* strain BB2000 reveals differences from the *P. mirabilis* reference strain. Genome Announc **1**(5)**:**e00024–13. http://dx.doi.org/10.1128/genomeA.00024-13.
44. **Pearson MM, Rasko DA, Smith SN, Mobley HLT.** 2010. Transcriptome of swarming *Proteus mirabilis*. Infect Immun **78:**2834–2845. http://dx.doi.org/10.1128/IAI.01222-09.
45. **Choi KH, Schweizer HP.** 2006. Mini-Tn7 insertion in bacteria with secondary, non-glmS-linked attTn7 sites: example *Proteus mirabilis* HI4320. Nature Protoc **1:**170–178. http://dx.doi.org/10.1038/nprot.2006.26.
46. **Maloy SR, Stewart VJ, Taylor RK.** 1996. Genetic analysis of pathogenic bacteria: a laboratory manual. Cold Spring Harbor Laboratory Press, Plainview, NY.
47. **Miller JH.** 1972. Experiments in molecular genetics. Cold Spring Harbor Laboratory Press, Cold Spring Harbor, NY.
48. **Grainger DC, Overton TW, Reppas N, Wade JT, Tamai E, Hobman JL, Constantinidou C, Struhl K, Church G, Busby SJ.** 2004. Genomic studies with *Escherichia coli* MelR protein: applications of chromatin immunoprecipitation and microarrays. J Bacteriol **186:**6938–6943. http://dx.doi.org/10.1128/JB.186.20.6938-6943.2004.
49. **Luo C, Lam E.** 2014. Quantitatively profiling genome-wide patterns of histone modifications in *Arabidopsis thaliana* using ChIP-seq. Methods Mol Biol **1112:**177–193. http://dx.doi.org/10.1007/978-1-62703-773-0_12.
50. **Luo C, Sidote DJ, Zhang Y, Kerstetter RA, Michael TP, Lam E.** 2012. Integrative analysis of chromatin states in *Arabidopsis* identified potential regulatory mechanisms for natural antisense transcript production. Plant J **73:**77–90. http://dx.doi.org/10.1111/tpj.12017.
51. **Hagberg L, Engberg I, Freter R, Lam J, Olling S, Svanborg Edén C.** 1983. Ascending, unobstructed urinary tract infection in mice caused by pyelonephritogenic *Escherichia coli* of human origin. Infect Immun **40:**273–283.
52. **Clemmer KM, Rather PN.** 2007. Regulation of *flhDC* expression in *Proteus mirabilis*. Res Microbiol **158:**295–302. http://dx.doi.org/10.1016/j.resmic.2006.11.010.
53. **Dufour A, Furness RB, Hughes C.** 1998. Novel genes that upregulate the *Proteus mirabilis flhDC* master operon controlling flagellar biogenesis and swarming. Mol Microbiol **29:**741–751. http://dx.doi.org/10.1046/j.1365-2958.1998.00967.x.
54. **Hay NA, Tipper DJ, Gygi D, Hughes C.** 1999. A novel membrane protein influencing cell shape and multicellular swarming of *Proteus mirabilis*. J Bacteriol **181:**2008–2016.
55. **Sturgill G, Rather PN.** 2004. Evidence that putrescine acts as an extracellular signal required for swarming in *Proteus mirabilis*. Mol Microbiol **51:**437–446. http://dx.doi.org/10.1046/j.1365-2958.2003.03835.x.
56. **Himpsl SD, Lockatell CV, Hebel JR, Johnson DE, Mobley HLT.** 2008. Identification of virulence determinants in uropathogenic *Proteus mirabilis* using signature-tagged mutagenesis. J Med Microbiol **57:**1068–1078. http://dx.doi.org/10.1099/jmm.0.2008/002071-0.
57. **Zunino P, Sosa V, Allen AG, Preston A, Schlapp G, Maskell DJ.** 2003. *Proteus mirabilis* fimbriae (PMF) are important for both bladder and kidney colonization in mice. Microbiology **149:**3231–3237. http://dx.doi.org/10.1099/mic.0.26534-0.
58. **Alamuri P, Mobley HLT.** 2008. A novel autotransporter of uropathogenic *Proteus mirabilis* is both a cytotoxin and an agglutinin. Mol Microbiol **68:**997–1017. http://dx.doi.org/10.1111/j.1365-2958.2008.06199.x.
59. **Walker KE, Moghaddame-Jafari S, Lockatell CV, Johnson D, Belas R.** 1999. ZapA, the IgA-degrading metalloprotease of *Proteus mirabilis*, is a virulence factor expressed specifically in swarmer cells. Mol Microbiol **32:**825–836. http://dx.doi.org/10.1046/j.1365-2958.1999.01401.x.
60. **Alteri CJ, Himpsl SD, Pickens SR, Lindner JR, Zora JS, Miller JE, Arno PD, Straight SW, Mobley HLT.** 2013. Multicellular bacteria deploy the type VI secretion system to preemptively strike neighboring cells. PLoS Pathog **9:**e1003608. http://dx.doi.org/10.1371/journal.ppat.1003608.
61. **Gibbs KA, Urbanowski ML, Greenberg EP.** 2008. Genetic determinants of self identity and social recognition in bacteria. Science **321:**256–259. http://dx.doi.org/10.1126/science.1160033.
62. **Wenren LM, Sullivan NL, Cardarelli L, Septer AN, Gibbs KA.** 2013. Two independent pathways for self-recognition in *Proteus mirabilis* are linked by type VI-dependent export. mBio **4**(4)**:**e00374–13. http://dx.doi.org/10.1128/mBio.00374-13.
63. **Lane MC, Li X, Pearson MM, Simms AN, Mobley HLT.** 2009. Oxygen-limiting conditions enrich for fimbriate cells of uropathogenic *Proteus mirabilis* and *Escherichia coli*. J Bacteriol **191:**1382–1392. http://dx.doi.org/10.1128/JB.01550-08.
64. **Feklistov A, Sharon BD, Darst SA, Gross CA.** 2014. Bacterial sigma factors: a historical, structural, and genomic perspective. Annu Rev Microbiol **68:**357–376. http://dx.doi.org/10.1146/annurev-micro-092412-155737.
65. **Browne JA, Harris A, Leir SH.** 2014. An optimized protocol for isolating primary epithelial cell chromatin for ChIP. PLoS One **9:**e100099. http://dx.doi.org/10.1371/journal.pone.0100099.
66. **Furness RB, Fraser GM, Hay NA, Hughes C.** 1997. Negative feedback from a *Proteus* class II flagellum export defect to the *flhDC* master operon controlling cell division and flagellum assembly. J Bacteriol **179:**5585–5588.
67. **Dillon SC, Dorman CJ.** 2010. Bacterial nucleoid-associated proteins, nucleoid structure and gene expression. Nat Rev Microbiol **8:**185–195. http://dx.doi.org/10.1038/nrmicro2261.
68. **Dorman CJ.** 2013. Co-operative roles for DNA supercoiling and nucleoid-associated proteins in the regulation of bacterial transcription. Biochem Soc Trans **41:**542–547. http://dx.doi.org/10.1042/BST20120222.
69. **Minchin SD, Busby SJ.** 2009. Analysis of mechanisms of activation and repression at bacterial promoters. Methods **47:**6–12. http://dx.doi.org/10.1016/j.ymeth.2008.10.012.
70. **Wade JT, Struhl K, Busby SJ, Grainger DC.** 2007. Genomic analysis of protein-DNA interactions in bacteria: insights into transcription and

chromosome organization. Mol Microbiol **65:**21–26. http://dx.doi.org/10.1111/j.1365-2958.2007.05781.x.
71. **Wiles TJ, Kulesus RR, Mulvey MA.** 2008. Origins and virulence mechanisms of uropathogenic *Escherichia coli*. Exp Mol Pathol **85:**11–19. http://dx.doi.org/10.1016/j.yexmp.2008.03.007.
72. **Pellegrino R, Scavone P, Umpiérrez A, Maskell DJ, Zunino P.** 2013. *Proteus mirabilis* uroepithelial cell adhesin (UCA) fimbria plays a role in the colonization of the urinary tract. Pathog Dis **67:**104–107. http://dx.doi.org/10.1111/2049-632X.12027.
73. **Ho BT, Dong TG, Mekalanos JJ.** 2014. A view to a kill: the bacterial type VI secretion system. Cell Host Microbe **15:**9–21. http://dx.doi.org/10.1016/j.chom.2013.11.008.
74. **Kapitein N, Mogk A.** 2013. Deadly syringes: type VI secretion system activities in pathogenicity and interbacterial competition. Curr Opin Microbiol **16:**52–58. http://dx.doi.org/10.1016/j.mib.2012.11.009.
75. **Russell AB, Peterson SB, Mougous JD.** 2014. Type VI secretion system effectors: poisons with a purpose. Nat Rev Microbiol **12:**137–148. http://dx.doi.org/10.1038/nrmicro3185.
76. **Belas R, Manos J, Suvanasuthi R.** 2004. *Proteus mirabilis* ZapA metalloprotease degrades a broad spectrum of substrates, including antimicrobial peptides. Infect Immun **72:**5159–5167. http://dx.doi.org/10.1128/IAI.72.9.5159-5167.2004.
77. **Phan V, Belas R, Gilmore BF, Ceri H.** 2008. ZapA, a virulence factor in a rat model of *Proteus mirabilis*-induced acute and chronic prostatitis. Infect Immun **76:**4859–4864. http://dx.doi.org/10.1128/IAI.00122-08.
78. **Bishop RE.** 2005. The lipid A palmitoyltransferase PagP: molecular mechanisms and role in bacterial pathogenesis. Mol Microbiol **57:**900–912. http://dx.doi.org/10.1111/j.1365-2958.2005.04711.x.
79. **Kovacs-Simon A, Titball RW, Michell SL.** 2011. Lipoproteins of bacterial pathogens. Infect Immun **79:**548–561. http://dx.doi.org/10.1128/IAI.00682-10.
80. **Ranallo RT, Kaminski RW, George T, Kordis AA, Chen Q, Szabo K, Venkatesan MM.** 2010. Virulence, inflammatory potential, and adaptive immunity induced by *Shigella flexneri msbB* mutants. Infect Immun **78:**400–412. http://dx.doi.org/10.1128/IAI.00533-09.
81. **Tan Y, Kagan JC.** 2014. A cross-disciplinary perspective on the innate immune responses to bacterial lipopolysaccharide. Mol Cell **54:**212–223. http://dx.doi.org/10.1016/j.molcel.2014.03.012.
82. **Balleza E, López-Bojorquez LN, Martínez-Antonio A, Resendis-Antonio O, Lozada-Chávez I, Balderas-Martinez YI, Encarnación S, Collado-Vides J.** 2009. Regulation by transcription factors in bacteria: beyond description. FEMS Microbiol Rev **33:**133–151. http://dx.doi.org/10.1111/j.1574-6976.2008.00145.x.
83. **Bonocora RP, Fitzgerald DM, Stringer AM, Wade JT.** 2013. Non-canonical protein-DNA interactions identified by ChIP are not artifacts. BMC Genomics **14:**254. http://dx.doi.org/10.1186/1471-2164-14-254.
84. **Fitzgerald DM, Bonocora RP, Wade JT.** 2014. Comprehensive mapping of the *Escherichia coli* flagellar regulatory network. PLoS Genetics **10:**e1004649. http://dx.doi.org/10.1371/journal.pgen.1004649.
85. **Jungwirth B, Sala C, Kohl TA, Uplekar S, Baumbach J, Cole ST, Pühler A, Tauch A.** 2013. High-resolution detection of DNA binding sites of the global transcriptional regulator GlxR in *Corynebacterium glutamicum*. Microbiology **159:**12–22. http://dx.doi.org/10.1099/mic.0.062059-0.
86. **Singh SS, Singh N, Bonocora RP, Fitzgerald DM, Wade JT, Grainger DC.** 2014. Widespread suppression of intragenic transcription initiation by H-NS. Genes Dev **28:**214–219. http://dx.doi.org/10.1101/gad.234336.113.
87. **Wade JT, Grainger DC.** 2014. Pervasive transcription: illuminating the dark matter of bacterial transcriptomes. Nat Rev Microbiol **12:**647–653. http://dx.doi.org/10.1038/nrmicro3316.
88. **Dorman CJ.** 2013. Genome architecture and global gene regulation in bacteria: making progress towards a unified model? Nat Rev Microbiol **11:**349–355. http://dx.doi.org/10.1038/nrmicro3007.
89. **Ko M, Park C.** 2000. H-NS-dependent regulation of flagellar synthesis is mediated by a LysR family protein. J Bacteriol **182:**4670–4672. http://dx.doi.org/10.1128/JB.182.16.4670-4672.2000.
90. **Lanois A, Jubelin G, Givaudan A.** 2008. FliZ, a flagellar regulator, is at the crossroads between motility, haemolysin expression and virulence in the insect pathogenic bacterium *Xenorhabdus*. Mol Microbiol **68:**516–533. http://dx.doi.org/10.1111/j.1365-2958.2008.06168.x.
91. **Mouslim C, Hughes KT.** 2014. The effect of cell growth phase on the regulatory cross-talk between flagellar and Spi1 virulence gene expression. PLoS Pathog **10:**e1003987. http://dx.doi.org/10.1371/journal.ppat.1003987.
92. **Guadarrama C, Medrano-Lopez A, Oropeza R, Hernandez-Lucas I, Calva E.** 2014. The Salmonella enterica serovar Typhi LeuO global regulator forms tetramers: residues involved in oligomerization, DNA binding, and transcriptional regulation. J Bacteriol **196:**2143–2154. http://dx.doi.org/10.1128/JB.01484-14.
93. **Lozada-Chávez I, Angarica VE, Collado-Vides J, Contreras-Moreira B.** 2008. The role of DNA-binding specificity in the evolution of bacterial regulatory networks. J Mol Biol **379:**627–643. http://dx.doi.org/10.1016/j.jmb.2008.04.008.